Biointerface Research in Applied Chemistry
Open-Access Journal (ISSN: 2069-5837)

Article
Volume 15, Issue 1, 205, 13
https://doi.org/10.33263/BRIAC151.013

Effect of NaOH Concentration on the Mechanical and Microstructural Properties of Fly Ash-Based Geopolymer

Dipankar Das [1,*], Prasanta Kumar Rout [1]

[1] Department of Material Science and Engineering, Tripura University (A Central University), Suryamaninagar, Agartala, Tripura-799022, India
* Correspondence: dipankar.msen@tripurauniv.in;

Scopus Author ID 57220885336
Received: 28.03.2024; 2.01.2025: date; Published: 12.02.2025

Abstract: This study offers a comprehensive investigation into the influence of varying NaOH concentrations on the mechanical and microstructural properties of Class F fly ash-based geopolymers. The activator solution used for this study was sodium hydroxide (NaOH) solution. The concentrations of NaOH solutions were kept at 6 Molars, 8 Molars, 10 Molars, 12 Molars, 14 Molars, and 16 Molars, respectively. The ratio of activator solution to fly ash powder was kept at 0.3, and the geopolymer specimens were cured at 60°C for 50 hours. After curing, mechanical properties such as compressive strength, flexural strength, and hardness values were determined. The fractured surface of geopolymer specimens was analyzed using FESEM, TEM, XRD, FTIR, etc. The water absorption test under tape water was conducted for 7, 14, and 28 days. The lowest water absorption of 7.46% was achieved within 28 days of curing. Further, the durability study of geopolymer specimens was conducted under high temperatures of 200°C, 400°C, 600°C, 800°C, and 1000°C, respectively. After exposure, the compression test of the exposed specimens was conducted to reveal the residual compressive strength. To study the microstructural properties, the fractured specimens after the mechanical test (compression test) were analyzed by using FESEM-EDS. Fly ash-based geopolymers have a wide range of potential applications across various fields such as construction and civil engineering, refractory and high-temperature applications, heritage and monument restoration, transportation infrastructure, marine and coastal applications, 3D printing, and advanced manufacturing fields, etc., due to their eco-friendliness, durability, and strong mechanical properties.

Keywords: fly ash; geopolymer; sodium hydroxide; compressive strength; FESEM.

1. Introduction

Due to various factors such as expeditious industrialization, urbanization, and population increase worldwide, electricity consumption is rapidly increasing. Coal-fired thermal power stations are an important source of electricity worldwide [1]. These power plants generate numerous amounts of fly ash powders as waste products after burning the pulverized coal in the boiler. Approximately 1.2 billion tonnes of fly ash are produced annually by coal-fired power stations worldwide [2]. Among them, roughly 64% of the fly ash is being used in various industries [3]. Many fly ash is discarded in dumpsites, where it often remains neglected. In many cases, these dumps are left uncovered, and as a result, fine fly ash particles can become airborne, leading to air pollution.

Additionally, the presence of numerous harmful substances can leach into the groundwater, contaminating it. This also pollutes the surrounding soils and disrupts the

structure of nearby plant communities [2,4-8]. Therefore, effectively disposing fly ash is desperately needed because it endangers human health and the environment. The components of the fly ash powders varied due to the source of coal being burned. The fly ash powder typically contains SiO_2, Al_2O_3, CaO, Fe_2O_3, etc., and some minor components [9]. According to ASTM C 618, these powders can be classed as type C or type F based on the proportion of CaO present [10]. The geopolymerization process emerged as the possible solution, where industrial solid waste materials can be utilized. Joseph Davidovits is one of the French materials scientists who coined the name "Geopolymer" in 1978 [11]. Geopolymers are a class of inorganic polymers that can be synthesized by aluminosilicate glassy source materials and an alkaline solution [12,13]. The geopolymers have exceptional mechanical properties such as compressive and flexural strength, rapid and low setting times, little shrinkage, fire and acid resistance, low thermal conductivity, and so on [12,14,15]. Geopolymer manufacture is cost-effective and affordable due to the availability of waste resources such as fly ash and the ease of the process. There are a number of stages associated with the geopolymer process. The first stage is the dissolution of silicates and aluminates, which takes place due to the activation of a highly alkaline solution, producing geopolymer gel; the second stage involves the hydrolysis process where silicate and aluminate tetrahedral units link with each other, and the third stage involves the polycondensation process followed by solidification of geopolymer gel and formation of three-dimensional aluminosilicate network [16].

The alkaline solution is one of the precursor materials required to form geopolymeric materials. It contributes significantly to the geopolymerization process by allowing Si and Al atoms from the source material to dissolve, resulting in the geopolymer specimen's mechanical properties [17,18]. The most common alkaline activators are sodium hydroxide (NaOH), potassium hydroxide (KOH), sodium silicate (Na_2SiO_3), potassium silicate (K_2SiO_3) solutions, or mixes of hydroxide and silicate solutions [19-21]. The concentration of alkaline solutions also plays a vital role in the mechanical strength of geopolymer products. It has been observed that the increase in concentration of an alkaline solution increases the compressive strength value, but after a certain concentration, the mechanical strength shows a reverse trend. The reverse trend of mechanical strength is due to the presence of the excess amount of OH^- ions disrupting the geopolymerization process [16,22,23]. Curing time and temperature are the other variables that influence mechanical strength, but adequate NaOH concentration shows greater effects on mechanical strength than curing conditions.

The fly ash-based geopolymer mortar and the effects of NaOH solutions on the properties of the materials were studied by Gorhan *et al*. [17]. The concentration of NaOH solutions was 3M, 6M, and 9M, where the curing temperature was maintained at 65°C and 85°C. It was observed that the curing process and porosity values are greatly affected by the concentration of NaOH solutions. The optimum compressive strength is achieved when the geopolymer specimens are prepared with 6M NaOH solutions and curing temperatures are 85°C. It was mentioned that while the physical parameters were not significantly affected, the compressive strength increased as the curing temperature rose. Abdullah *et al*. [24] studied the fly ash-based geopolymer specimen where the concentration of NaOH solutions was 6, 8, 10, 12, 14, and 16 molars, the ratio of solid to liquid was 1.5, 2.0, 2.5, and the ratio of Na_2SiO_3 to NaOH is maintained at 0.5, 1.0, 1.5, 1.5, 2.0, 2.5, and 3.0, respectively. The optimum condition for fly ash-based geopolymer is 12 molars (NaOH solutions), 2.0 (solid to liquid ratio), and 2.5 (Na_2SiO_3 to NaOH ratio). The maximum compressive strength of 71.04 MPa was obtained after curing at 60°C. Chindaprasirt *et al*. [25] studied the fly ash-based geopolymer concrete,

where the concentration of NaOH solutions was 8-18 molars with intervals of 2 molars. It was reported that the increase in the concentration of NaOH solutions increases the compressive strength after fixed curing in air for 28 days. The prepared geopolymer specimens were also exposed to seawater in Thailand for 3 years, and it was observed that specimens that were prepared with a high concentration of NaOH solutions gained strength as compared with specimens prepared with a low concentration. Ghafoor *et al*. [26] studied the locally available fly ash-based geopolymer concrete with a NaOH concentration of 8 to 16 molar, liquid-to-solid ratio of 0.4 to 0.6, and the ratio of Na_2SiO_3 to NaOH maintained at 1.5 to 2.5. The ambient curing condition was opted for the geopolymer concrete. The geopolymer specimen prepared with the 14M NaOH solution shows the highest compressive strength of 21.5 MPa, whereas the highest flexural strength of 5 MPa was achieved with 16M NaOH solutions. The optimum ratio of Na_2SiO_3 to NaOH and liquid to solid was 1.5 and 0.5, respectively. The effects of NaOH solutions on fly ash and rice husk-based geopolymer were studied by Hwang *et al*. [27]. It was reported that the geopolymer specimen prepared with 35% rice husk ash with 10M NaOH solutions attributed to the highest compressive strength of 35.4 MPa. Therefore, it can be concluded that the mechanical properties of the geopolymer specimen are significantly influenced by the process parameters.

This present research aims to investigate the effects of NaOH concentration on fly ash-based geopolymer properties such as compressive strength, flexural strength, and hardness value. The fractured geopolymer specimens are characterized by FESEM, TEM, XRD, FTIR, and TGA-DTA, respectively. The water absorption test under tape water was conducted for 7, 14, and 28 days. To examine the thermal stability, the geopolymer specimen that obtains the highest mechanical strength is exposed to high temperatures of 200℃, 400℃, 600℃, 800℃, and 1000℃, respectively. After exposure, the residual compressive strength of the exposed specimen was obtained using a digital compression testing machine, and the fractured specimens were analyzed using the FESEM analysis.

2. Materials and Method

The starting raw material (Fly ash) was provided by National Thermal Power Corporation Limited (NTPC), Bongaigaon, India, and is a byproduct of coal-based thermal power plants. The elements of fly ash powder were determined using X-ray fluorescence (XRF). An optical microscope (model: DM 750M, make: Leica) and Carl Zeiss make FESEM equipped with EDS (model: Sigma-300) is used to observe the micrograph of the fly as powder. The fly ash powder is dispersed in ethanol and distributed above the glass slide to obtain the particle morphology under an optical microscope. In this present study, sodium hydroxide solutions were used as alkaline solutions. To prepare the sodium hydroxide solutions, the NaOH pellets are mixed with distilled water in a conical flask and kept at room temperature for 24 hours to get stable solutions. The concentration of sodium hydroxide is maintained at 6 molars (M), 8 molars (M), 10 molars (M), 12 molars (M), 14 molars (M), and 16 molars (M), respectively. The proportion of liquid to solid was maintained at 0.3. The fly ash powder and sodium hydroxide solution were mixed manually in a plastic container for 5-10 minutes during the processing. The geopolymer paste was cast in a cylindrical mold and vibrated by hands for 2-5 minutes. After ambient curing for 24 hours, the geopolymer samples are removed from the mold and cured artificially in a hot air oven at 60℃ for 50 hours. Further, the artificially cured specimens are stored at room temperature for testing and analysis. Table 1 lists the mixed design of geopolymer paste. The sample ID 6MGP, 8MGP, 10MGP, 12MGP, 14MGP, and

16MGP indicate geopolymer specimens are prepared with 6, 8, 10, 12, 14, and 16 molar NaOH solutions. Aimil India Limited made AIM-314E-DG-1 model digital compression testing equipment used to test the compressive strength of cured geopolymer specimens and flexural strength was tested using the Hieco make HL 590 model universal testing machine. The hardness of geopolymeric specimens was tested using a ZwickRoell make JS-TANGO model Vickers microhardness testing machine. The fractured geopolymer specimens' microstructures were characterized using FESEM equipment (model: Carl Zeiss Sigma-300), and Jeol makes TEM equipment (model- 2100F). Before being exposed to the FESEM, the samples are coated with gold using gold sputter equipment. Further, before exposure to TEM equipment, the fly ash and geopolymer specimen powder are dispersed in ethanol with the help of sonication, and a drop of diluted suspension is poured onto a copper grid with the help of an injection. The fractured specimens were also analyzed using PANalytical to make XRD (model- X'Pert PRO) and Bruker to make FTIR (model- Alpha T), respectively. PerkinElmer TGA-DTA equipment (model- PYRIS Diamond) was used for the thermal analysis of the 14MGP specimen. The TGA was used to check the sample's mass loss, and phase transformation analysis was analyzed by DTA simultaneously. A 20 mg powder of fractured geopolymer specimen was heated from room temperature to 900℃, where the heating rate was 10℃/minute. The flow chart of fly ash-based geopolymer specimen preparation is shown in Figure 1. Table 1 shows the mix design of geopolymer paste.

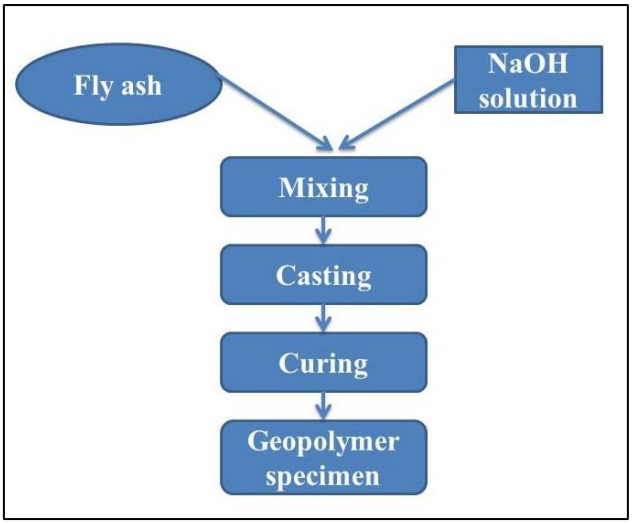

Figure 1. Flow of chart of geopolymer specimen preparation.

Table 1. Mix design of geopolymer paste.

Sl. No.	Sample ID	Raw materials	Molarity (M) of NaOH solution	Liquid (activator)/ solid (fly ash powder) ratio	Curing temperature (℃) and time
1	6MGP	Fly ash	6	0.3	60℃ and 50 hours
2	8MGP	Fly ash	8	0.3	
3	10MGP	Fly ash	10	0.3	
4	12MGP	Fly ash	12	0.3	
5	14MGP	Fly ash	14	0.3	
6	16MGP	Fly ash	16	0.3	

Note: Sample ID 6MGP denotes that the geopolymer sample was prepared with 6 molars of sodium hydroxide solution and so on.

3. Result and Discussions

The detailed characterizations of as-received fly ash powders are published by Das *et al*. [28]. Figure 2 shows the oxide compositions of fly ash powders. Figure 2 shows that the

sum of SiO2 and Al2O3 is about 84.5%, indicating that these fly ash powders belong to Class F type as described in ASTM C618 [10,29,30]. CaO and Fe_2O_3 are present in the fly ash powders at 1.59% and 5.91%, respectively. Along with major elements, minor elements such as TiO_2, MgO, ZnO, SO_3, SrO, K_2O, and Na_2O are also present in the fly ash powder.

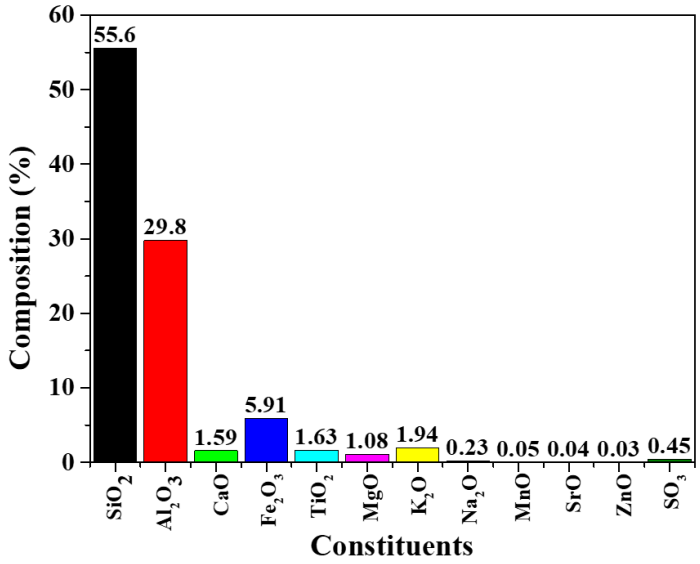

Figure 2. Chemical compositions of fly ash powder.

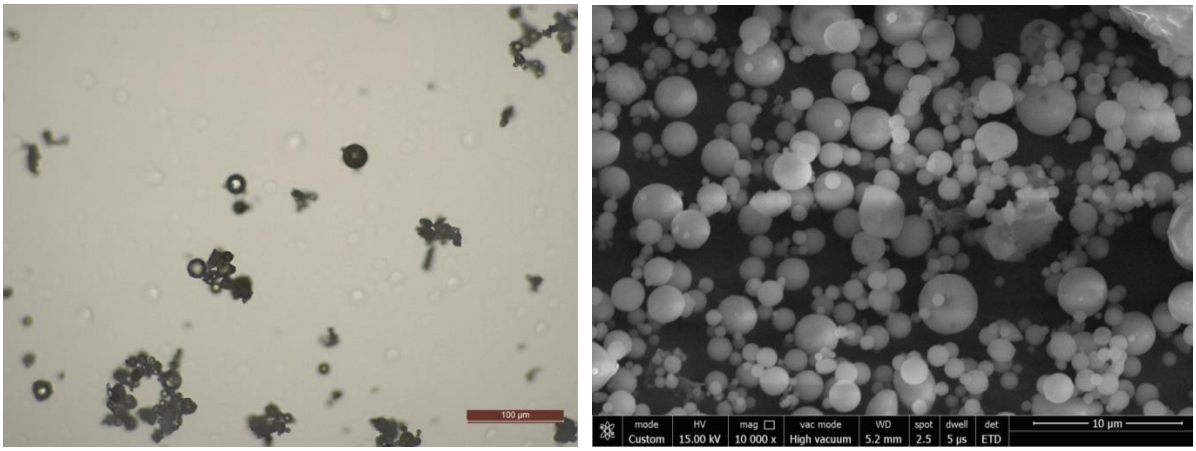

(a) **(b)**

Figure 3. Morphology of fly ash powder under **(a)** Optical microscope; **(b)** SEM microscope.

The optical microscope images and SEM morphology of fly ash powders are shown in Figure 3. From both the figures, it can be observed that fly ash powders are spherical in shape and of various sizes. Few powders are not spherical, and few are angular in shape. The agglomeration of fly ash particles with each other is also observed. Figure 4 illustrates the elemental mapping of fly ash powder. The mapping images of fly ash powder show the distribution of various elements in starting materials. The powders contain the distribution of Si, Al, and O as major elements and minor element distribution of Ca, Fe, Ti, Mg, and Mn, respectively.

To calculate the bulk density of the geopolymer specimens, the height and diameter of cylindrical geopolymeric specimens were measured by Vernier caliper, and Essae-Teraoka Private Limited make's weight measuring instrument was used to determine the weights of the specimens. The following formula was used to calculate the bulk density, where M and V represent the mass and volume of the specimens.

$$\text{Bulk Density } \left(\frac{g}{cc}\right) = \frac{M}{V} \text{ [31]}$$

Table 2 lists the bulk densities of geopolymer specimens. From the table, it can be observed that the geopolymer specimen ID 6MGP, 8MGP, 10MGP, 12MGP, 14MGP, and 16MGP show the bulk density (g/cc) of 1.56 g/cc, 1.59 g/cc, 1.63 g/cc, 1.83 g/cc, 2.05 g/cc, and 1.98 g/cc, respectively. A minimum of three specimen densities were measured, and their average is reported in this study.

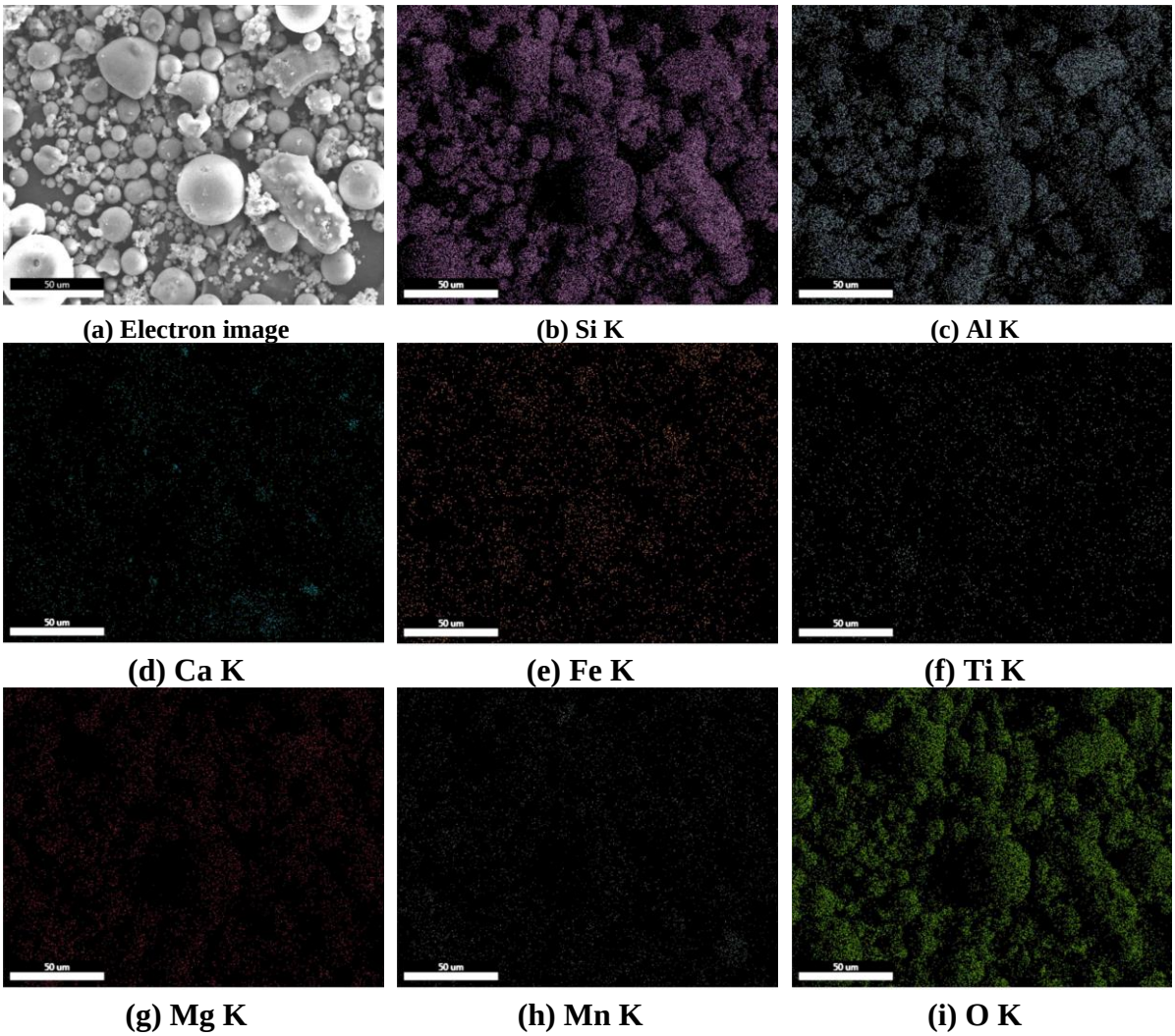

Figure 4. SEM and element mapping of fly ash powder **(a)** SEM micrograph in BSE mode; **(b)** Si distribution; **(c)** Al distribution; **(d)** Ca distribution; **(e)** Fe distribution; **(f)** Ti distribution; **(g)** Mg distribution; **(h)** Mn distribution; **(i)** O distribution.

Table 2. Bulk density of geopolymer specimens.

Sl. No.	Sample ID	Molarity (M) of NaOH solution	Density (g/cc)
1	6MGP	6M	1.56
2	8MGP	8M	1.59
3	10MGP	10M	1.63
4	12MGP	12M	1.83
5	14MGP	14M	2.05
6	16MGP	16M	1.98

Figure 5 (a-c) illustrates the variation of mechanical properties, including compressive strength, flexural strength, and hardness value of geopolymer specimens prepared with different NaOH concentrations. The mechanical properties of the geopolymer specimen increase with the increase of NaOH concentration for up to a certain concentration, i.e., 14M, but show a reverse trend after that. The sample ID 6MGP achieved the lowest compressive strength of 4 MPa, whereas the sample ID 8MGP, 10MGP, 12MGP, and 14MGP achieve the

compressive strength of 10 MPa, 16 MPa, 25 MPa, and 32 MPa, respectively. The sample (16MGP) prepared with the 16 molars NaOH solutions shows a less compressive strength of 27 MPa than the sample ID 14MGP. Figure 5(b) shows that the sample ID 6MGP, 8MGP, 10MGP, 12MGP, 14MGP, and 16MGP exhibits the flexural strength of 0.96 MPa, 1.2 MPa, 3.0 MPa, 4.7 MPa, 6.3 MPa, and 5.0 MPa, respectively. The microhardness value in Figure 5(c) shows that the sample ID 14MGP achieved the highest value of 67.84 HV. The reasons for the good mechanical strength are fly ash's reactivity and high alkaline solutions. It has been observed that the lower concentration of NaOH solutions gives lower strength due to weak chemical reactions. Further, it retards the rate of the geopolymerization process [22]. The declinations of mechanical strength after 16 molar NaOH concentrations are due to the presence of excess OH^- ions, which increases the dissolution of silica and alumina from fly ash powder but hinders the polycondensation process. The amorphous sodium aluminosilicate hydrate (N-A-S-H) gel is the primary and main reaction product of the geopolymerization reaction [32-34]. The formation of this gel in the geopolymer results in the high-strength geopolymer. Still, the aluminosilicate gel precipitation occurs at the early stages when the OH─ ions exceed requirements, which results in the lower compressive strength of geopolymer specimens. Somna *et al*. [35] studied the fly ash-based geopolymer with NaOH concentrations of 4.5, 7.0, 9.5, 12.0, 14.0, and 16.5 molars, where the liquid-to-solid ratio is maintained at 0.3. The specimens were cured under ambient curing conditions. It was reported that the mechanical properties and microstructure of the geopolymer specimen are greatly dependent on the concentration of NaOH solutions.

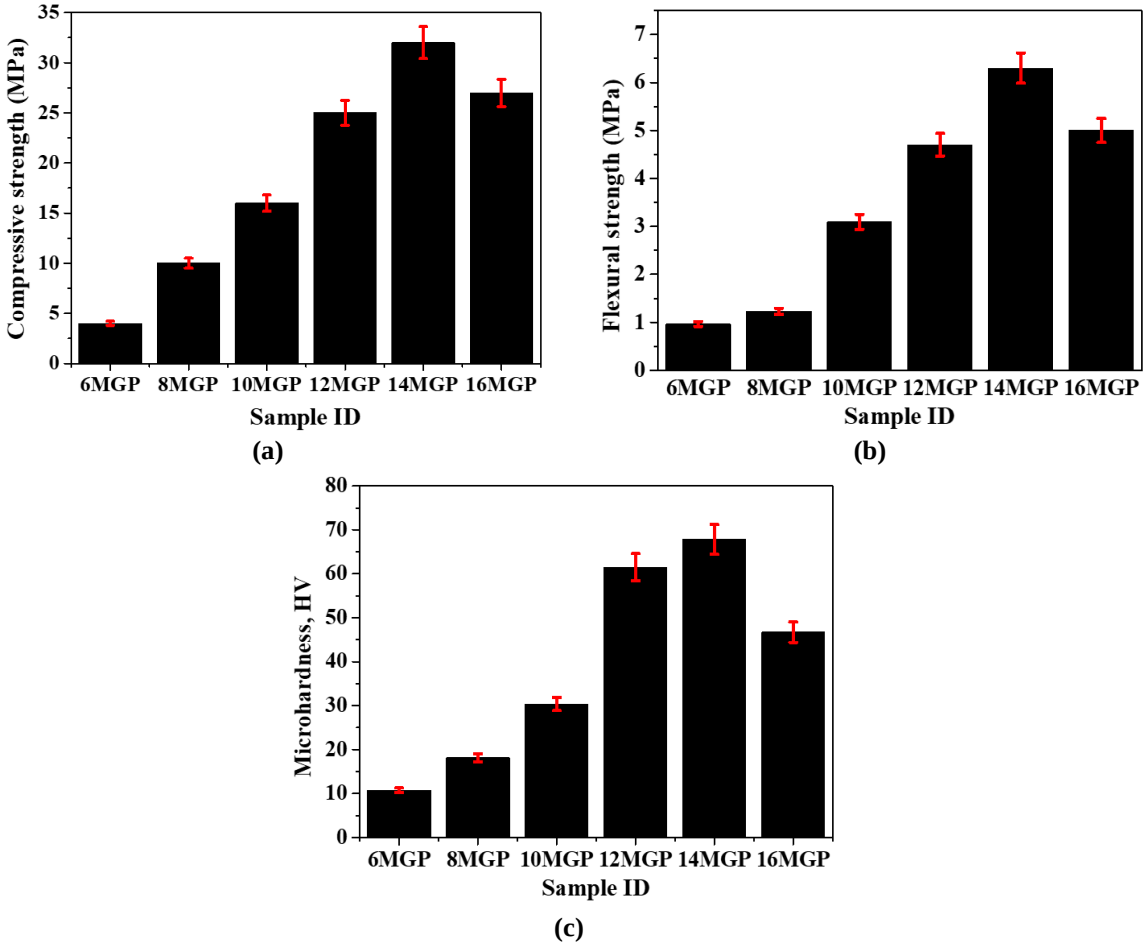

Figure 5. Mechanical properties of fly ash-based geopolymer: **(a)** Compressive strength; **(b)** Flexural strength; **(c)** Microhardness.

The geopolymer specimen's compressive strength increased noticeably when the NaOH concentration was raised from 4.5 molars to 14 molars, but after that, the strength showed a reverse direction. The highest compressive strength of 25.5 MPa was achieved with 60 days of ambient curing. It was also reported that the low concentration of NaOH solutions shows low reactivity at ambient curing conditions [36].

Additionally, due to the high concentration of NaOH solutions, the release of alumina and silica takes place, yielding to the geopolymer gel followed by polymerization and hardening, resulting in excellent mechanical strength. Hanjitsuwan *et al*. [37] studied the high calcium fly ash-based geopolymer paste with NaOH concentrations of 8, 10, 12, 15, and 18 molars. It was reported that the concentration of NaOH solutions substantially impacted the mechanical and electrical characteristics of the geopolymer paste. Further, it was also reported that the high concentration of NaOH solutions increases the leaching of Si and Al from the starting raw materials, which results in a high degree of geopolymerization process attributed to the setting time and mechanical strength. The maximum compressive strength of 56 MPa was achieved with 18 molars of NaOH concentration. The fly ash-based geopolymer mortar was studied by Pavithra *et al*. [38], where the concentration of NaOH was maintained at 10 to 18 molars with intervals of 2 molars. The NaOH concentration of 16 molars with the ratio of Na_2SiO_3 to NaOH of 1.5 exhibits the highest compressive strength of around 45 MPa. However, the increase in NaOH concentration leads to a decrease in compressive strength.

Figures 6 (a, c, e, g, i, k) reveal the fractured surface of a geopolymer specimen prepared with varied concentrations of 6M, 8M, 10M, 12M, 14M, and 16M, respectively. This surface was studied by using FESEM equipment. With an increase in NaOH concentration, the diffusion rate of fly ash powder increases, which can be observed in Figures 6(a, c, e, g). It exhibits an inhomogeneous structure and particles that have undergone partial and complete reactions. The microstructure also shows some pores. Figure 6(a) exhibits that most fly ash powders are not reacted, where the 6 molar NaOH solutions were used. This reveals that 6 molar NaOH solutions are not enough to diffuse the fly ash powders. The samples in which most particles have not participated in the reaction mechanism are due to the lack of sufficient concentration of NaOH solutions. The low interaction of fly ash particles with NaOH solutions leads to the formation of an insufficient amount of aluminosilicate gel, which results in low mechanical strength [38]. Figures 6(c, e, g) exhibit that with increased NaOH solutions, the fly ash powders show reactivity and result in partially and fully reacted particles with N-A-S-H gel. Figure 6(i) shows the SEM fractograph of geopolymer specimen ID 14MGP. The samples prepared with the 14 molars NaOH solutions show a densely compacted microstructure and few unreacted, partially fly ash particles. It also shows few pores and micro-cracks in the sample. Further, it can be seen that the microstructure of sample ID 16MGP is porous with long micro-cracks, and few fully and partially unreacted particles are also observed. Gao *et al*. [18] reported that the dissolution of silicate and aluminate from starting raw materials due to the activation of high concentrations of NaOH solutions helps the polycondensation process, leading to excellent mechanical strength. Further, a few authors also reported that the excess amount of NaOH results in the quick setting of geopolymer paste, but it decreases the mechanical strength [38]. The EDS analysis of geopolymer prepared with NaOH concentrations of 6M, 8M, 10M, 12M, 14M, and 16M concentrations are shown in Figure 6 (b,d,f,h,j,l). The EDS spectra predominantly exhibit the presence of Si, Al, Na, and O components. This suggests the production of N-A-S-H gel, resulting in a compacted matrix with high mechanical strength [39,40].

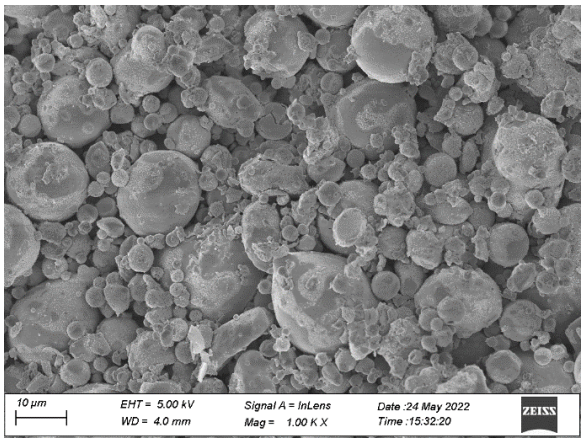
10 µm
EHT = 5.00 kV
WD = 4.0 mm
Signal A = InLens
Mag = 1.00 K X
Date :24 May 2022
Time :15:32:20
ZEISS

(a)

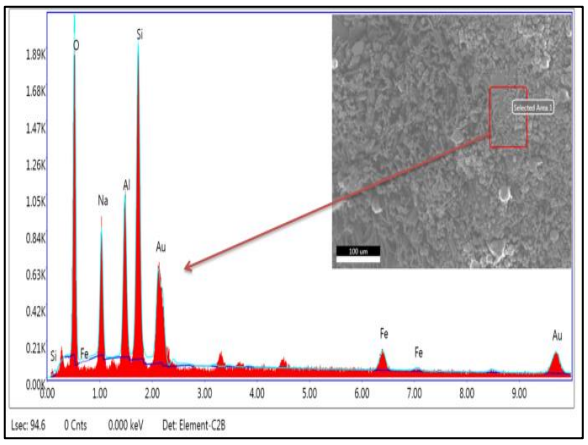
O
Si
Na
Al
Au
Fe
Fe
Au
Lsec: 94.6
0 Cnts
0.000 keV
Det: Element-C2B

(b)

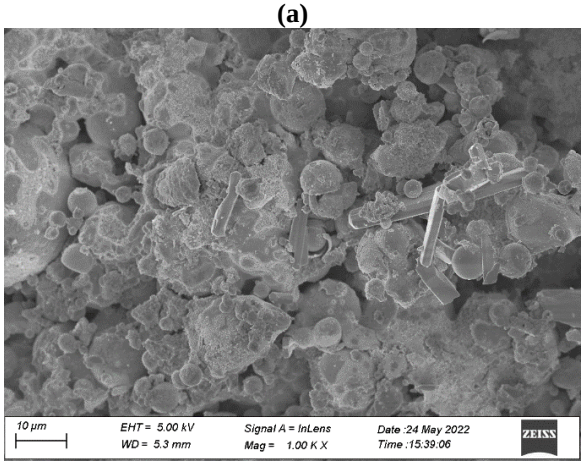
10 µm
EHT = 5.00 kV
WD = 5.3 mm
Signal A = InLens
Mag = 1.00 K X
Date :24 May 2022
Time :15:39:06
ZEISS

(c)

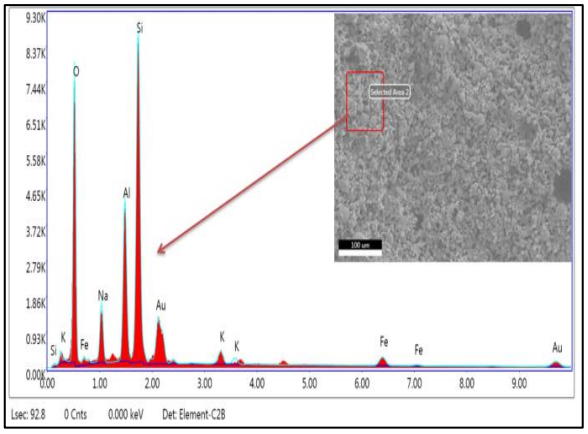
O
Si
Al
Na
Au
K
Fe
Fe
Au
Lsec: 92.8
0 Cnts
0.000 keV
Det: Element-C2B

(d)

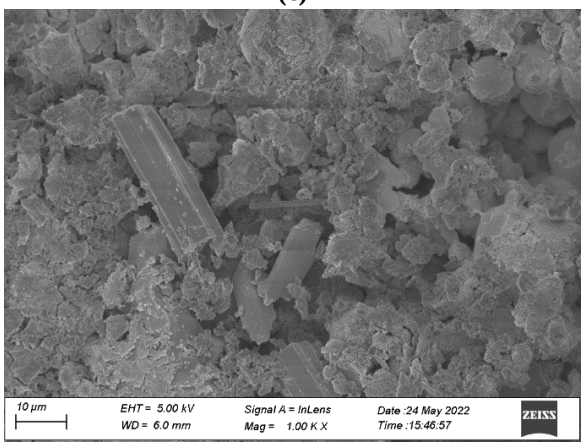
10 µm
EHT = 5.00 kV
WD = 6.0 mm
Signal A = InLens
Mag = 1.00 K X
Date :24 May 2022
Time :15:46:57
ZEISS

(e)

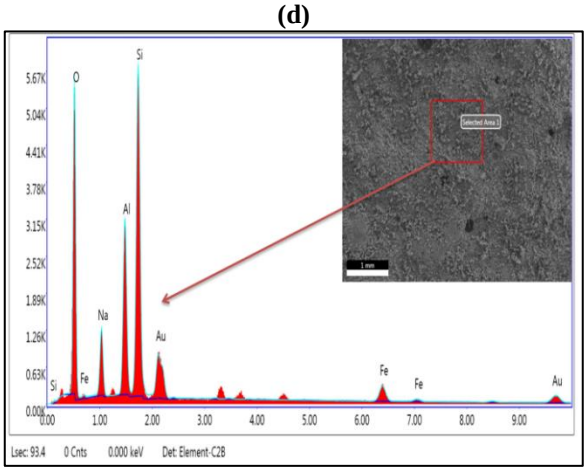
O
Si
Al
Na
Au
Fe
Fe
Au
Lsec: 93.4
0 Cnts
0.000 keV
Det: Element-C2B

(f)

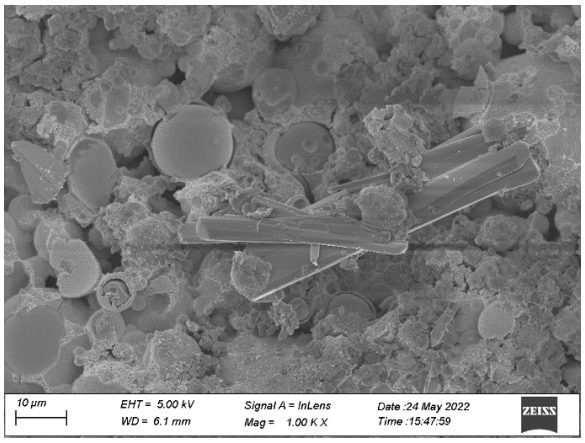
10 µm
EHT = 5.00 kV
WD = 6.1 mm
Signal A = InLens
Mag = 1.00 K X
Date :24 May 2022
Time :15:47:59
ZEISS

(g)

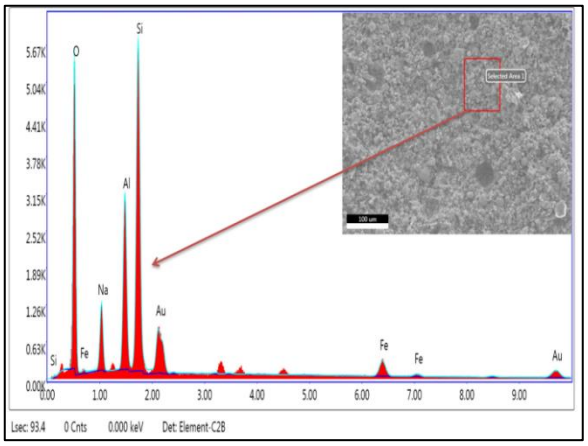
O
Si
Al
Na
Au
Fe
Fe
Au
Lsec: 93.4
0 Cnts
0.000 keV
Det: Element-C2B

(h)

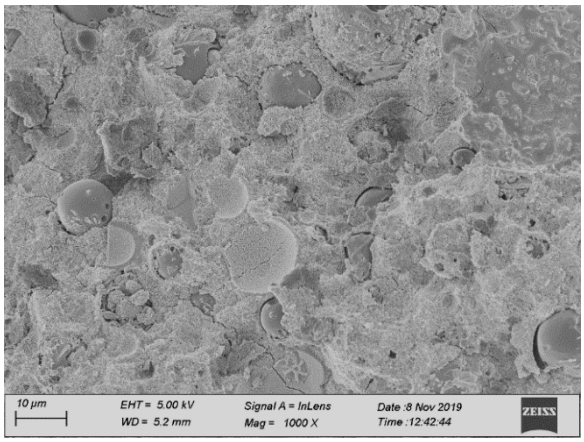

(i)

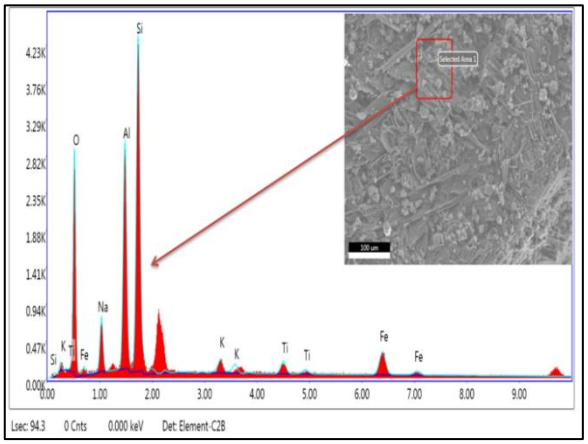

(j)

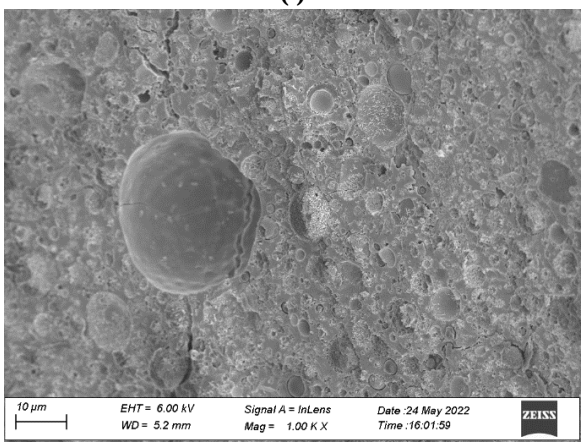

(k)

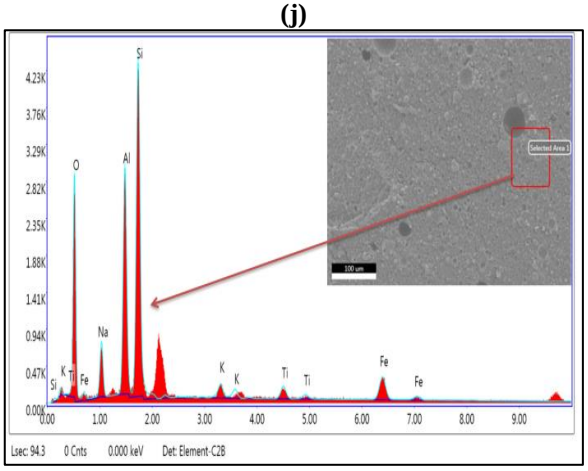

(l)

Figure 6. Representative SEM fractographs and EDS analysis of geopolymer specimen **(a,b)** 6MGP; **(c,d)** 8MGP; **(e,f)** 10MGP; **(g,h)** 12MGP; **(i,j)** 14MGP; **(k,l)** 16MGP.

Figure 7 represents the elemental mapping of the optimized geopolymer specimen ID 14MGP. The distribution of various elements on the surface can be seen from the mapping images.

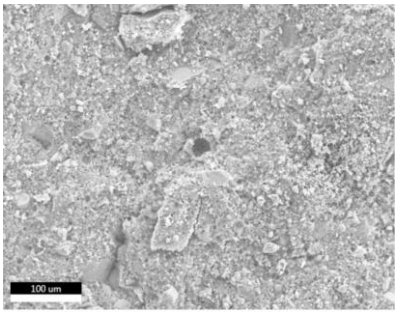

(a) Electron image

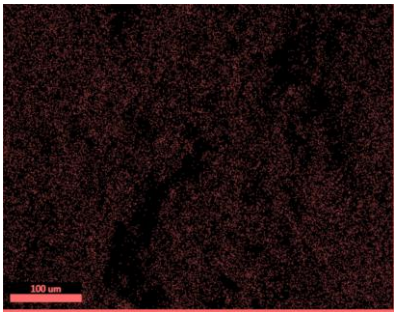

(b) Si K

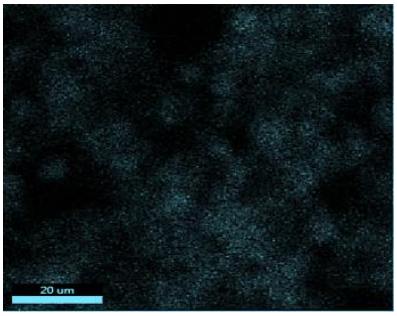

(c) Al K

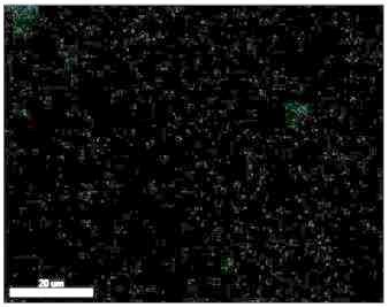

(d) Ca K

(e) Fe K

(f) Zn K

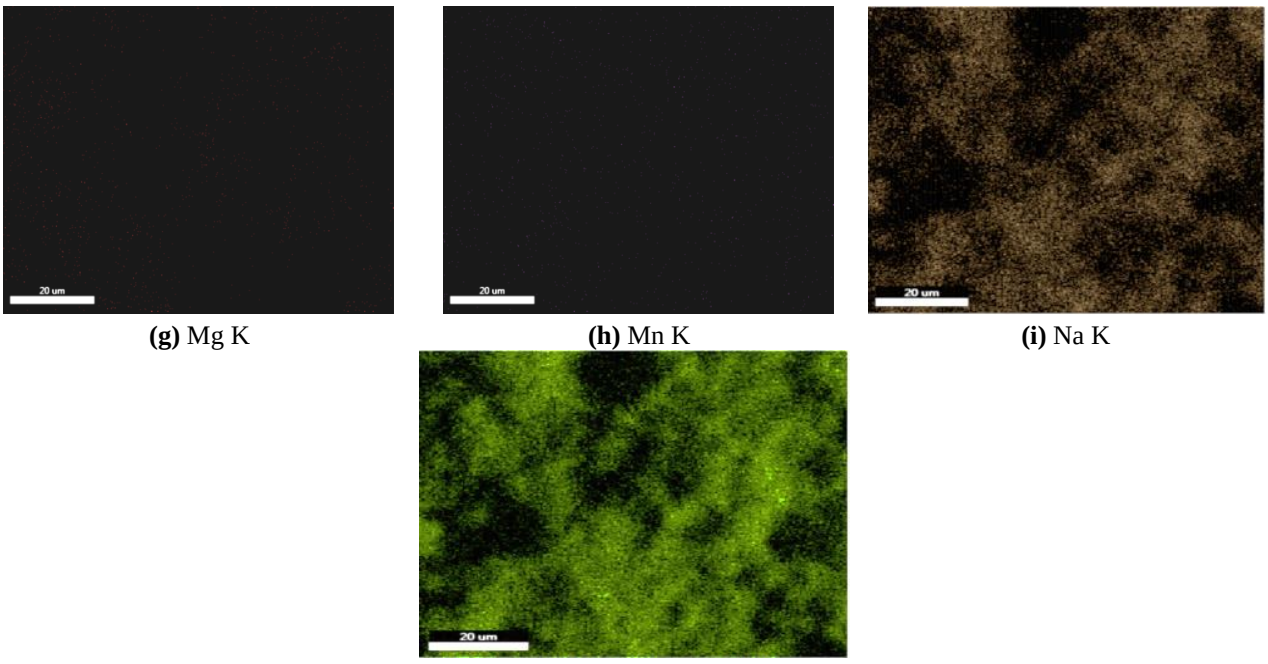

(g) Mg K **(h)** Mn K **(i)** Na K

(j) O K

Figure 7. SEM and element mapping of geopolymer specimen ID 14MGP: **(a)** SEM micrograph in BSE mode; **(b)** Si distribution; **(c)** Al distribution; **(d)** Ca distribution; **(e)** Fe distribution; **(f)** Zn distribution; **(g)** Mg distribution; **(h)** Mn distribution; **(i)** Na distribution; **(j)** O distribution.

Transmission electron microscopy was used to look more closely at the topography of the fly ash powders and the geopolymer sample's microstructural characteristics. Figure 8(a) shows the TEM micrographs of fly ash powder. From the micrographs, it can be observed that most of the particles are spherical, and few are angular. The agglomeration of particles can also be observed on the surface. Other researchers made the same observation [41,42]. Figure 8(b) displays the distinctive transmission electron microscopy images of the geopolymer sample with the identification code of 14MGP. The activation of fly ash powders with an alkaline activator of 14 molar NaOH solution forms a geopolymer gel. Other researchers have also confirmed the formation of geopolymer gel [34,43,44]. The figure reveals that a few parts are dark, a few parts are light white, and a few parts are completely white. The darker parts indicate the formation of a compacted geopolymer matrix. In contrast, the light white parts are the geopolymer gel, and the completely white parts are the pores of the geopolymer specimens. The similar observations are consistent with those of other researchers [43].

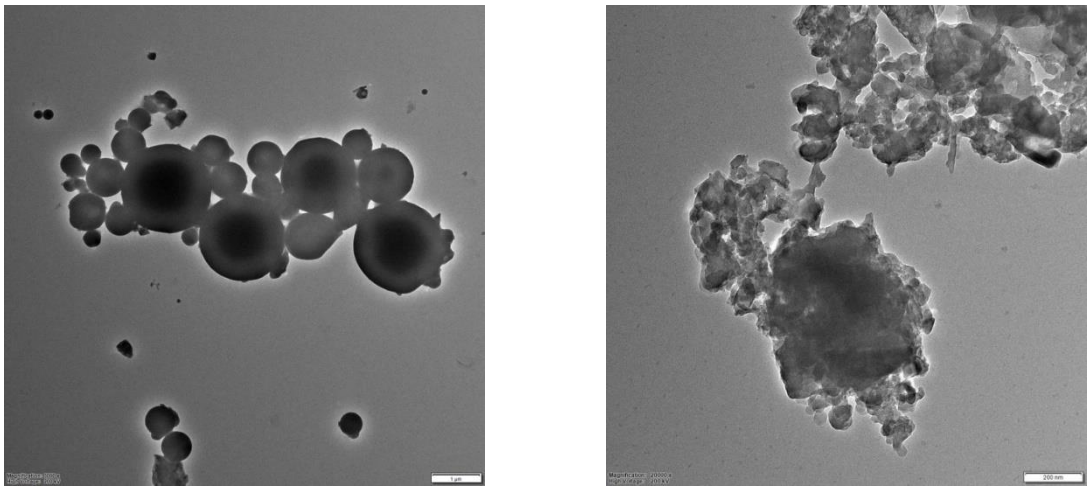

(a) **(b)**

Figure 8. Transmission electron microscopy of **(a)** fly ash powder; **(b)** geopolymer specimen ID 14MGP.

The FTIR spectra of fly ash powder and the geopolymeric specimen synthesized by the various concentrations of NaOH solutions are represented in Figure 9. The IR spectrum of fly ash powders shows various peaks at 463, 733, and 799 cm^{-1}, which are associated with the Si-O-Si bending vibration, symmetric stretching vibrations of Si-O-Al, and symmetric stretching vibrations of Si-O-Si, respectively. The intense band at 1073 cm^{-1} is associated with the asymmetric stretching vibrations of Si-O-Si and Si-O-Al [34]. The peaks at 1553 and 1647 cm^{-1} are attributed to the stretching vibration of O-C-O and the bending vibrations of H-O-H. From the FTIR spectra graph, it can be seen that after activation of fly ash powder by various concentrations such as 6, 8, 10, 12, 14, and 16 molars of NaOH solutions, the main intense peak at 1073 cm^{-1} of fly ash powders is shifted to the lower wavenumbers (cm^{-1}). The shifting of the peak from higher to lower wave numbers indicates some chemical changes that happened due to the activation of fly ash by various concentrations of NaOH solutions, and new products are formed. The shifting of peaks from higher to lower wavenumbers and the formation of new products are consistent with the results of other researchers [27,34,35]. The band in the region of 1611 to 1666 cm^{-1} wavenumbers and 3412 to 3573 cm^{-1} wavenumbers is associated with the bending vibrations of H-O-H and stretching vibrations of OH, respectively [27,45,46].

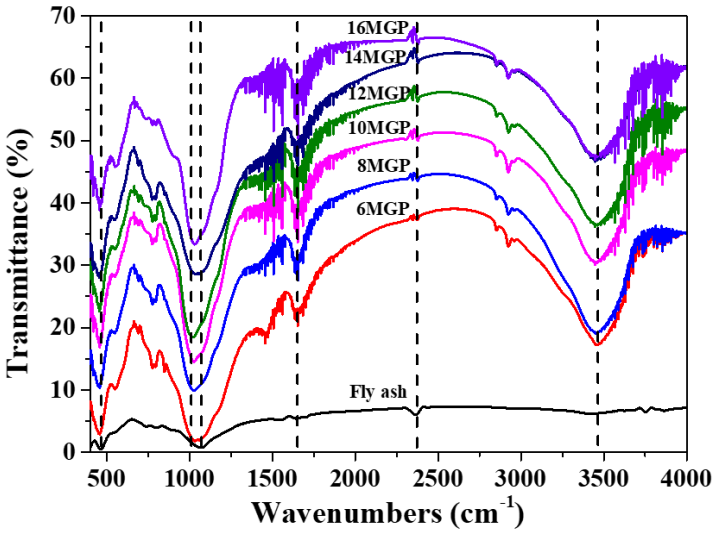

Figure 9. FTIR spectra of geopolymer specimen.

The X-ray diffraction analysis of fly ash powder and the geopolymer specimens synthesized by various concentrations of NaOH solutions such as 6M, 8M, 10M, 12M, 14M, and 16 M are shown in Figure 10. It is observed that the fly ash powder used in this present investigation is mainly comprised of crystalline phases, namely quartz and mullite phases. A broad hump was observed at a low angle of 18° to 35° in the 2 theta region, indicating the presence of an amorphous phase in the materials. The presence of an amorphous phase at a low angle is consistent with the results of other researchers [46-48]. The XRD pattern revealed no alumina peaks, which indicates that the alumina presence in the starting raw materials is primarily in the amorphous phase [27]. The XRD pattern of the geopolymer specimen prepared with the various concentrations of NaOH solutions such as 6, 8, 10, 12, 14, and 16 molars is also shown along with the XRD pattern of parent materials. It was observed from the XRD pattern that the number of characteristic peaks present in the starting raw materials remained the same in geopolymer specimens after the geopolymerization process. Quartz and mullite are the two main crystalline phases found in geopolymeric specimens, which form the main mineral framework attributed to the mechanical strength of the geopolymeric specimen. However, the intensity of the peaks is increased or decreased compared to the peaks of parent

materials. Hwang *et al*. [27] and Liew *et al*. [49] reported that the decrease of peak intensity is related to the dissolution of the starting raw materials into the inorganic polymeric materials. The broad hump at 2Ɵ regions of the geopolymer specimen is slightly flattened as compared to the hump of parent materials. Davidovits [50] and Teng *et al*. [51] reported that this diffuse halo is a typical characteristic of sodium aluminosilicate geopolymer gels.

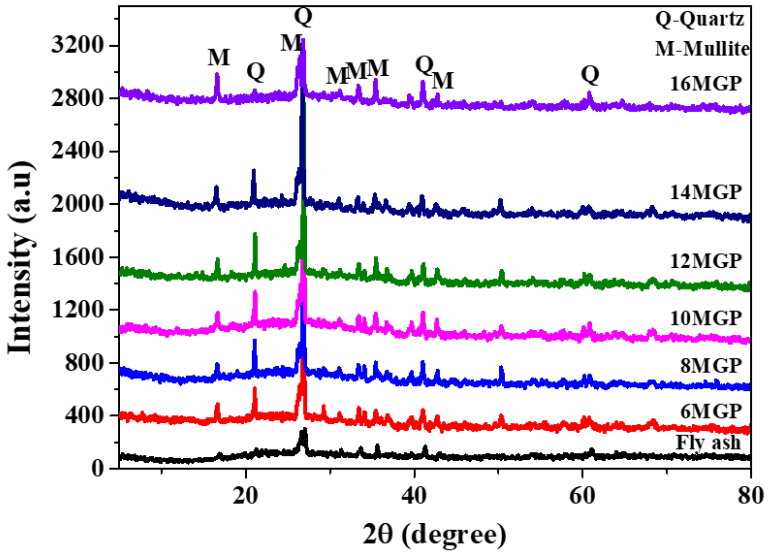

Figure 10. XRD analysis of geopolymer specimen.

The water absorption ability of any construction material is a significant feature that affects the material's durability. Table 3 shows the water absorption (%) of geopolymer specimens. The specimen that achieved the highest mechanical strength (optimized specimen) was taken for a water absorption test.

Table 3. Water absorption (%) of geopolymer specimens.

Sl. No.	Days	Sample ID	Sample 1	Sample 2	Sample 3	Mean water absorption (%)
1	7	14MGP	9.88	9.52	9.87	9.75
2	14	14MGP	8.86	8.27	8.98	8.70
3	28	14MGP	7.79	7.62	6.98	7.46

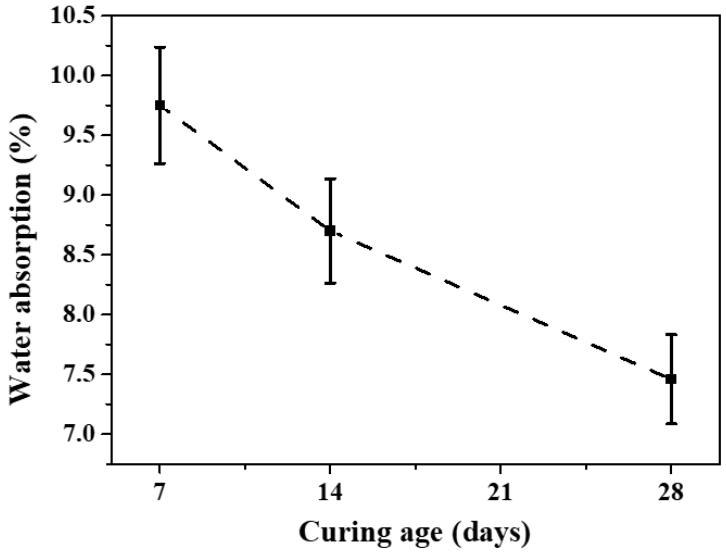

Figure 11. Water absorption rate (%) graph of geopolymer specimen.

A minimum of three specimens are immersed in water for the water absorption test, and their average values are reported in this present investigation. From the table, it can be shown that the geopolymer specimen 14MGP was immersed for 7, 14, and 28 days, revealing the water absorption of 9.75%, 8.70%, and 7.46%, respectively. Figure 11 shows the graph between water absorption percent and curing age in days. The graph exhibits the reduction of the water absorption rate with increased curing days. If the geopolymer specimen absorbs lower water, then it can be said that this material shows excellent resistance to water penetration. Excellent water penetration to materials results in lower environmental damage to the materials. Farhana *et al*. [52] reported that the increase in curing time (days) for water absorption reduces the pore size, which results in the specimen's structure becoming denser and harder. Rashad *et al*. [53] studied the fly ash-based geopolymer mortar with sea sand, and it was reported that the increase in curing days reduces the water absorption rate due to the reduction of pore size.

The optimized geopolymer specimen ID 14MGP, which achieved the highest mechanical strength, is exposed to high temperatures of 200℃, 400℃, 600℃, 800℃, and 1000℃ in a muffle furnace to check the thermal stability. Before being exposed to elevated temperatures, the sharp edges of geopolymeric specimens were finished with emery paper to avoid crack propagation. The heating rate on the muffle furnace was 5℃/ minute. The soaking time of the geopolymer specimen was 1 hour, and the specimens were cooled inside the furnace. After cooling, the specimens are kept at room temperature, followed by compression testing using a digital compression testing machine. Figure 12(a) shows the muffle furnace equipment, and 12(b) shows the heating curve of geopolymer specimen ID 14MGP under various temperatures.

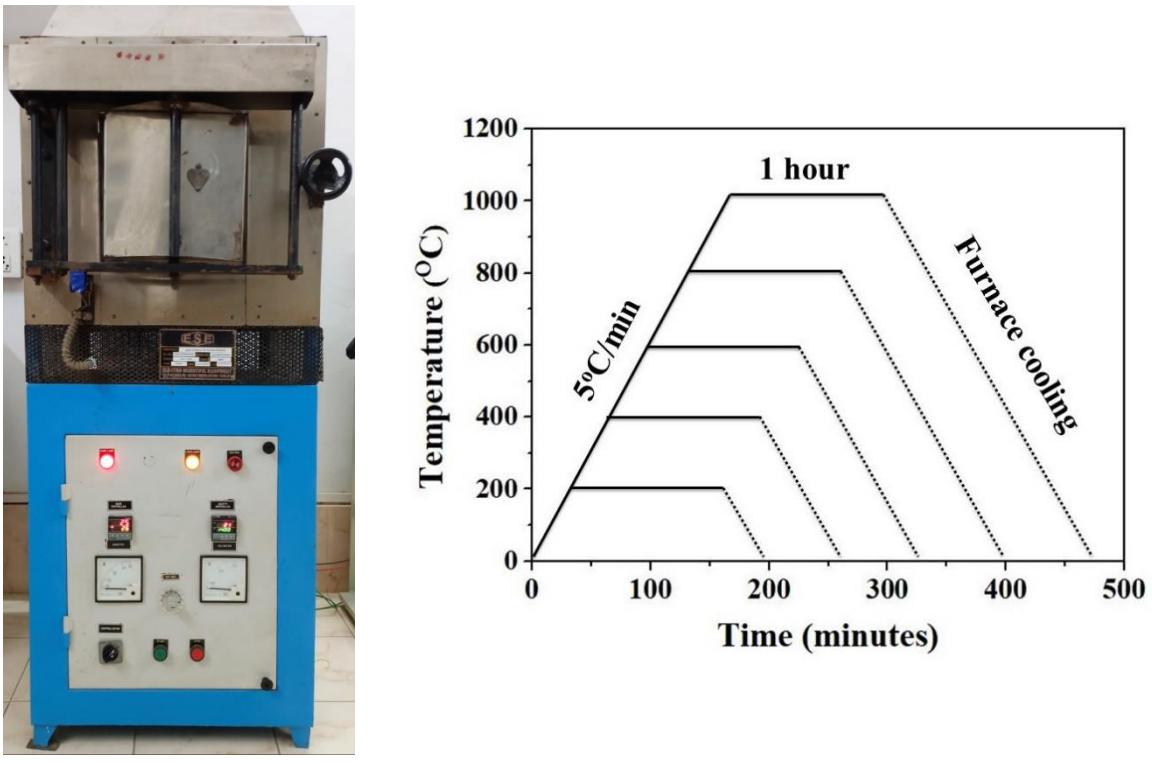

(a) **(b)**

Figure 12. (a) Muffle furnace equipment; **(b)** Heating curve of geopolymer specimen ID GP14M under various temperatures.

The surfaces of the geopolymer specimen before and after exposure to the elevated temperatures are shown in Figure 13 (a-f). The figure shows that after exposure to elevated

temperatures, the color of the geopolymer specimen surface has significantly changed compared to the surface before exposure. The gradual temperature changes subjected to geopolymeric specimens result in a change of color. It can be observed that after exposure to 600℃, 800℃, 900℃ and 1000℃, the geopolymer specimen colors change from grey to reddish or rusty color due to the chemical compositions of the starting raw materials, i.e., fly ash powders. The presence of Fe_2O_3 % is around 5.91 % in the raw materials, and its oxidation due to high temperature is the main reason for the rusty color [54].

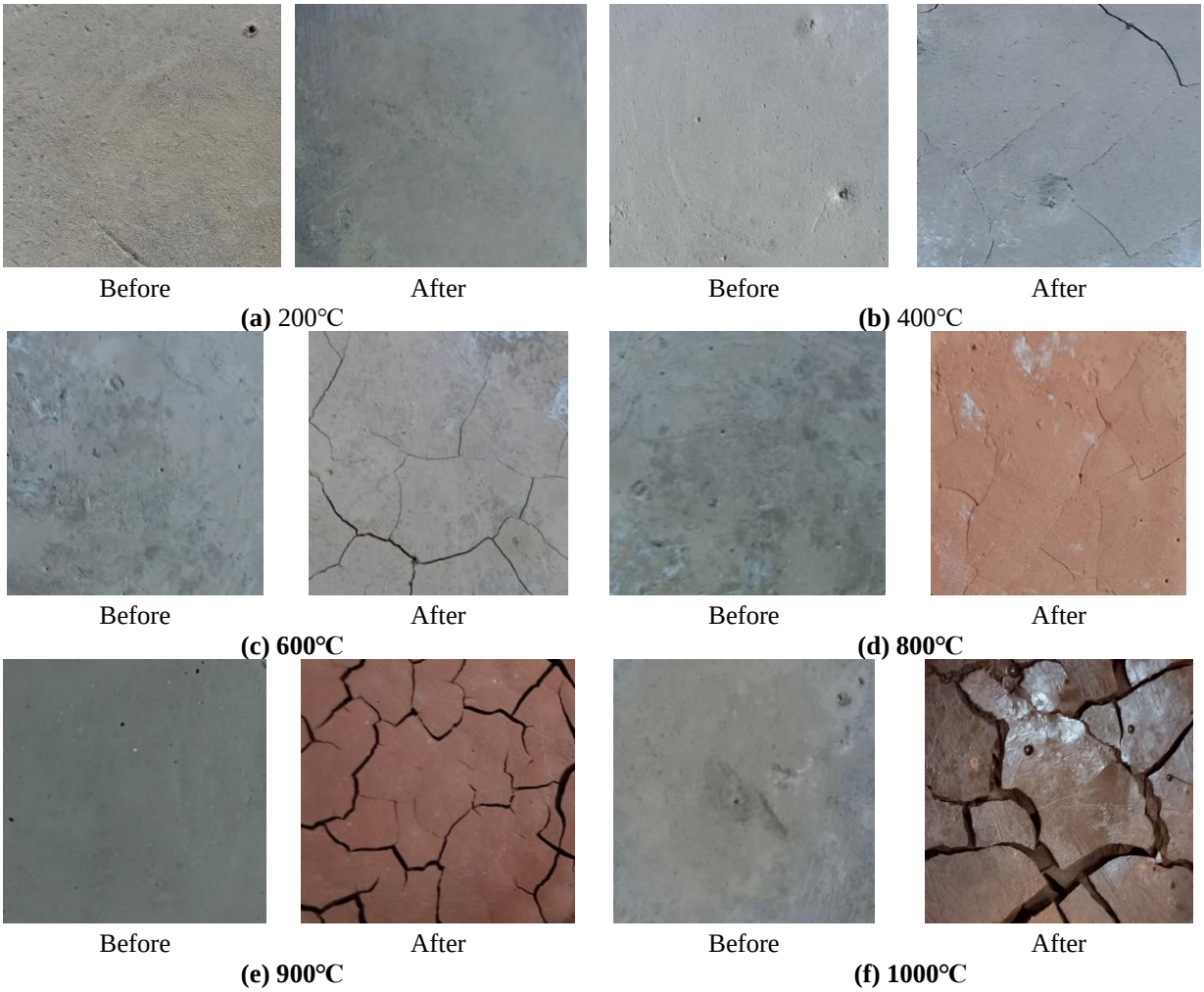

Figure 13. The surface of the geopolymer specimen before and after exposure to the high temperature: **(a)** 200℃; **(b)** 400℃; **(c)** 600℃; **(d)** 800℃; **(e)** 900℃; **(f)** 1000℃.

The bulk density (g/cc) of geopolymer specimens ID 14MGP and the specimens after exposure to high temperatures are tabulated in Table 4. A minimum of three specimen's densities were measured, and their averages were reported in this present investigation.

Table 4. Bulk density (g/cc) of geopolymer specimens ID GP14M.

Sl. No.	Sample ID	Temperature (°C)	Density (g/cc)
1	GP14M (Before exposure)	------	1.89
2	GP14M (After exposure)	200	1.70
3	GP14M (After exposure)	400	1.62
4	GP14M (After exposure)	600	1.59
5	GP14M (After exposure)	800	1.54
6	GP14M (After exposure)	1000	1.52

TGA-DTA analysis graph of fly ash powder and reference geopolymer specimen ID 14MGP is shown in Figure 14. PerkinElmer-based TGA-DTA instrument PYRIS Diamond

TG-DTA model was used to check the thermal stability of the geopolymer specimen, where the specimens are heated up to 900°C. The heating rate for the analysis was 10°C/minute. After mechanical testing, the fractured geopolymer specimens were powdered, and 20 mg of powder was weighed using a measuring instrument for analysis. From Figure 14(a), it can be observed that the mass loss of fly ash powder is around 4%. The mass loss of the powders can be attributed to the fraction of volatile compounds present, which can be determined during the heating of the powders. The DTA curve of fly ash powder shows various peaks at around 50°C, 115°C, 244°C, 367°C, 495°C, and 773°C, respectively. These peaks are associated with the removal of freely and weakly bound water molecules from the raw materials. The same type of observation was also observed by Nergis *et al*. [55]. The mass loss of geopolymer powder samples when heated from room temperature to 900°C was measured using TGA. Figure 14(b) shows the TGA-DTA graph of the 14MGP specimen. From the TGA graph, it can be observed that the highest mass loss is 11% when the specimens are heated up to 200°C. The mass loss is attributed to the weakly bonded water molecules and evaporable free waters that are released from geopolymeric specimens at temperatures below 200°C [56]. After 200°C, when the specimens are exposed to much higher temperatures, the curve of mass loss gradually decreases. The similar observations are consistent with the other researchers [57,58]. From the DTA curve of geopolymer specimen ID 14MGP, it can be observed that at 80°C, one sharp endothermic peak is present, which is attributed to the loss of the free water from the aluminosilicate gel of the geopolymeric specimen. The free water loss from the geopolymer specimen below 100°C is consistent with other researchers' observations [57,59]. The exothermic hump in the range of 500°C to 700°C is due to the existence of unburnt carbon [60]. Nergis *et al*. [55] studied the fly ash, sand, and glass powder-based geopolymer materials where it was reported from the DTA curve that the free and weakly bound water molecules are removed in the region of 123 to 130, 185, 232 to 240, 312 to 358, 490 to 497, and 572 to 576°C, due to heat exposure. It was also reported that the water in the geopolymeric materials could be found in various forms, such as hygroscopic or free water (up to 120°C), strong physically bonded water (120-300°C), and chemically bound water (above 300°C), respectively.

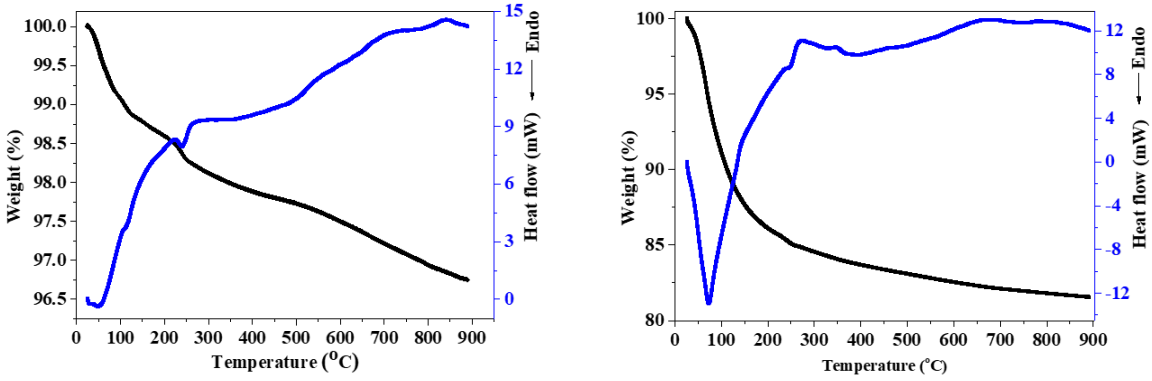

Figure 14. TGA-DTA graph of **(a)** fly ash powder; **(b)** geopolymer specimen ID 14MGP.

Table 5 shows the residual compressive strength of the reference geopolymer specimen ID 14MGP after exposure to various temperatures. It can be observed from the table that the reference geopolymer specimen ID 14MGP shows a compressive strength of 32 MPa before exposure to the elevated temperature; however, when the reference specimens are exposed to elevated temperatures such as 200, 400, 600, 800, and 1000°C show residual compressive strength of 34.2, 30.1, 25.0, 10.5, and 0 MPa, respectively. From the table, it can be observed that after exposure to 200°C, the compressive strength of the geopolymer specimen has been

increased slightly, which may be due to the presence of high temperature, which further initiates the geopolymerization process and results in dense structure as compared to the reference geopolymer specimen. The same observation was also reported in the previous studies [61-63]. The specimens exposed to a temperature above 200°C show a reduction in compressive strength. The exposure of specimens to elevated temperatures induced severe thermal stress because of the evaporation of water from the geopolymer structure, which causes cracks to form [64]. The compressive strength was significantly decreased by these cracks. The geopolymer specimen exposed to 1000°C shows a compressive strength of 0 MPa, which may be due to excessive moisture loss resulting in the initiation of cracks in the geopolymer specimen. The formation of cracks in the specimen reduces the compressive strengths. Payakaniti *et al*. [65] studied the fly ash-based geopolymer specimen under elevated temperatures and reported that the reference geopolymer specimen shows a compressive strength of 57.4 MPa, which increases the compressive strength up to 71 MPa after exposure to 200°C. It was also reported that after 400°C, the compressive strength declines. The strength decline is attributed to the thermal stress, which results in the cracks. Kuri *et al*. [61] studied the ferronickel slag and fly ash-based geopolymer mortar under elevated temperatures, where it was reported that the residual compressive strength increased when exposed to 200°C, but a further increase in temperature lowered the strength. The reduction of strength is attributed to the movement of chemically and physically bonded water as well as the OH groups, the phase transformation of geopolymers, the generation of anhydrous products, and the sintering process [66,67]. The fly ash and waste rubber-based geopolymer concrete under high temperatures was studied by Luhar *et al*. [68]. Rubberized geopolymer concrete and control geopolymer concrete are exposed to 200, 400, 600, and 800°C, and it was observed that after exposure up to 600°C, the compressive strength is reduced. The fly ash and waste rubber-based geopolymer concrete specimens exposed to 800°C show a slight improvement in compressive strength.

Table 5. Residual compressive strength (MPa) of geopolymer specimens ID GP14M.

Sl. no	Specimen ID	Description	Residual compressive strength (MPa)
1	14MGP	Specimen cured at 60°C for 50 hours (reference specimen)	32
2	14MGP	200°C	34.2
3	14MGP	400°C	30.1
4	14MGP	600°C	25.0
5	14MGP	800°C	10.5
6	14MGP	1000°C	0

Figure 15 shows the SEM image of the fractured surface of geopolymer specimen ID 14MGP after exposure to elevated temperatures of 200°C (a,b), 400°C (c,d), 600°C (e,f), 800°C (g,h), and 1000°C (i,j), respectively. From Figure 15(a-b), it can be observed that the microstructural characteristics are dense and homogeneous structures with few unreacted and partially reacted particles. After exposure to 200°C, the geopolymer specimens show a slight increment of mechanical properties, which may be due to further initiation of geopolymerization reaction due to temperature. Some parts of the specimen show geopolymer gel along with a few micro pores and micro-cracks. The formation of geopolymer gel due to efficient geopolymerization reaction results in a compacted structure. This compacted structure leads to excellent mechanical strength, which can be observed from the compressive strength data. Micro-cracks development is attributed to water's evaporation during the curing periods and after exposure to 200°C. Other researchers reported the same observation [69,70]. The

fractograph (Figure 15c,d, 15e,f) of geopolymer specimens exposed to 400 and 600°C also shows few unreacted, partially reacted particles and voids on the surface, which may be formed due to evaporation of weakly bonded water molecules. The number of voids or pores increased after exposure to 400 and 600°C and became connected, followed by the formation of cracks, which are mainly responsible for reducing mechanical strength. The microstructure of the geopolymer specimens, which are exposed to 800°C, is shown in Figure 15(g,h). The fractograph reveals a few unreacted, partially reacted particles along with voids and cracks on the surface of the specimen. The formation of cracks in the specimen is due to the high pressure formed inside the specimen when exposed to the high temperature. A partial dissolution of leftover particles can be observed from the surface of the geopolymer specimen. The fractographs of geopolymer specimens exposed to the elevated temperatures of 1000°C are shown in Figure 15(i,j). The figure reveals that all the particles are partially and fully fused due to high-temperature exposure and form larger voids and cracks in the specimen due to high pressure, dehydration, and dihydroxylation. Ahmari *et al*. [71] reported that the geopolymeric structures are deformed as a result of the dihydroxylation. These voids and cracks are connected in the geopolymer specimen, which is attributed to the more randomly distributed micro-cracks and results in the further deterioration of compressive strengths. The reduction of compressive strength after exposure to 1000°C is consistent with observations of other researchers [56,69]. The EDS spectra of geopolymer specimen after exposure to elevated temperatures of 200°C, 400°C, 600°C, 800°C, and 1000°C are shown in Figure 16(a-e).

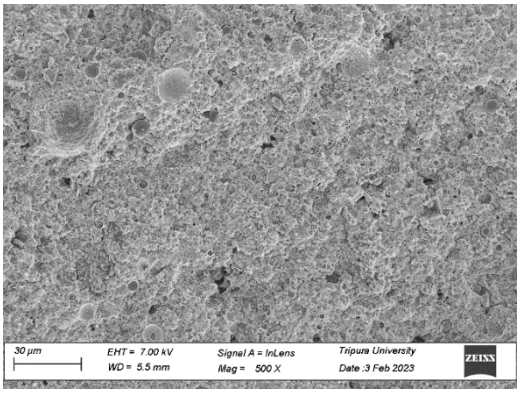

(a)

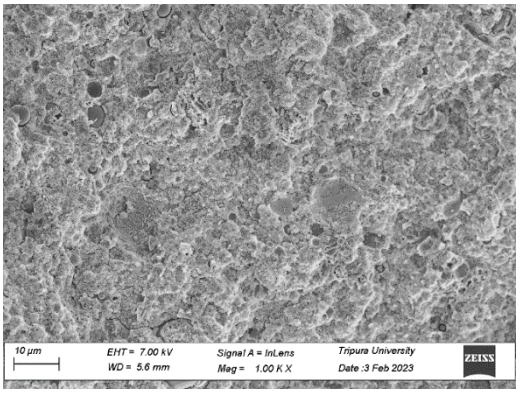

(b)

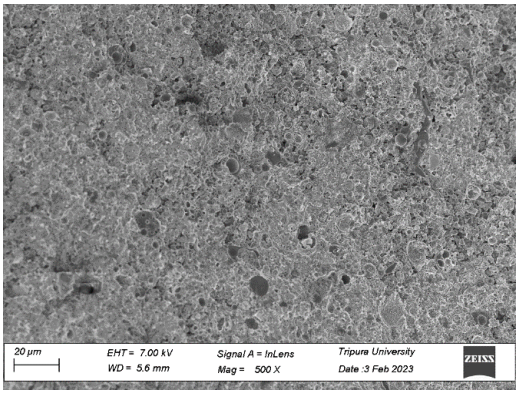

(c)

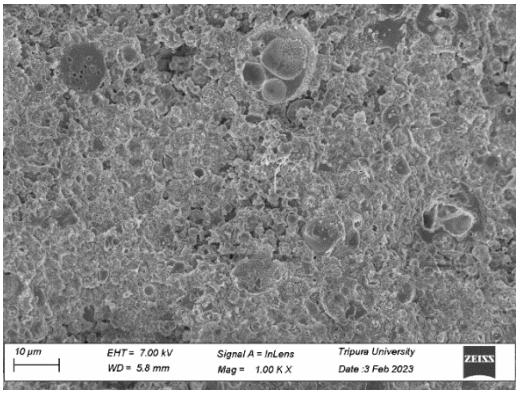

(d)

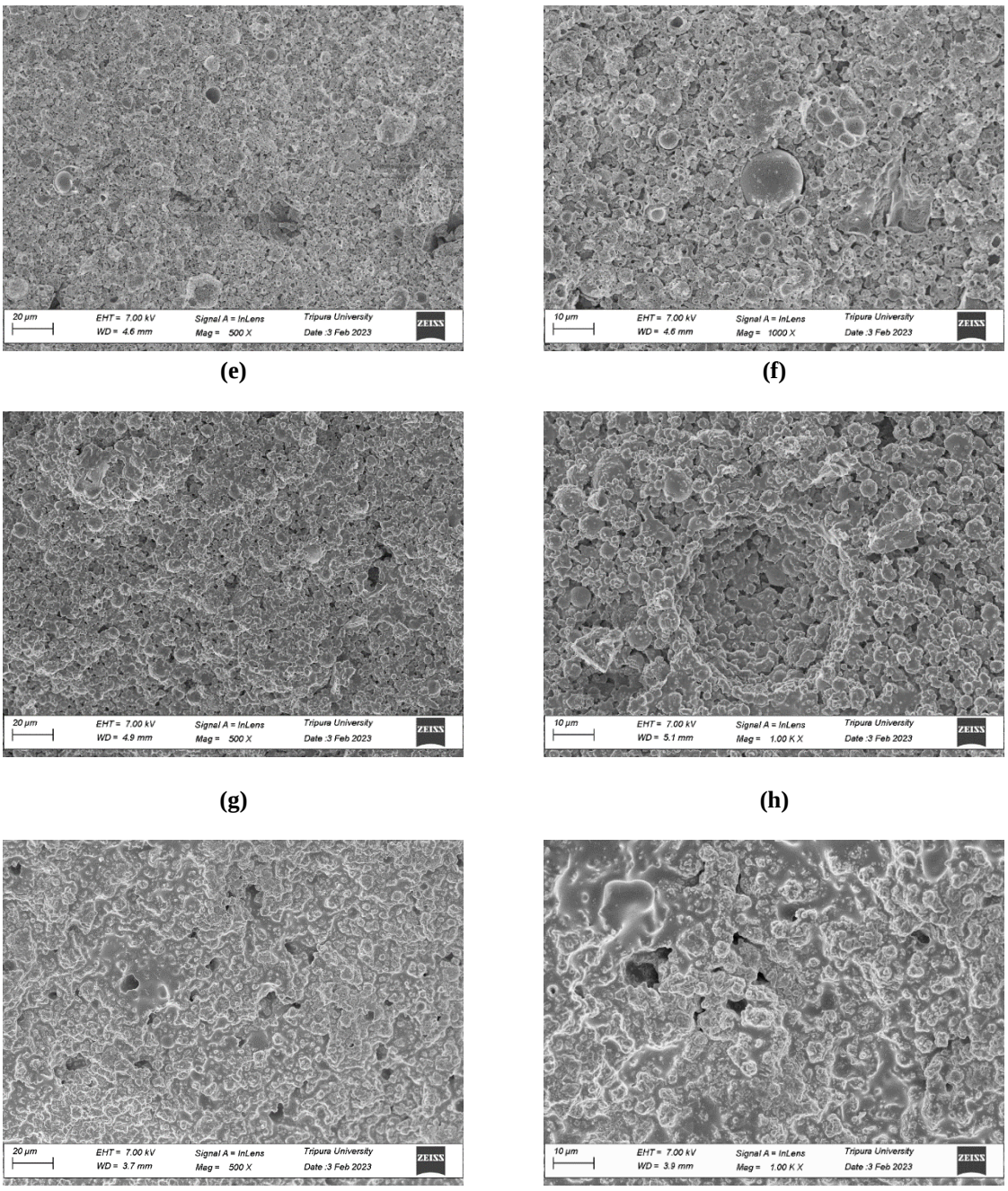

Figure 15. SEM image of a fracture surface of geopolymer specimen ID 14MGP under exposure to high temperature: **(a,b)** 200°C; **(c,d)** 400°C; **(e,f)** 600°C; **(g,h)** 800°C; **(i,j)** 1000 C, respectively.

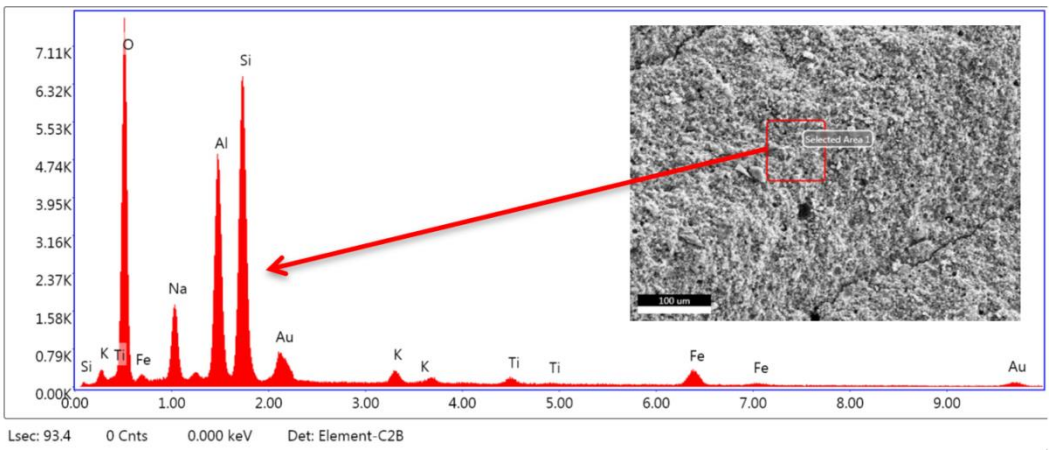

(a)

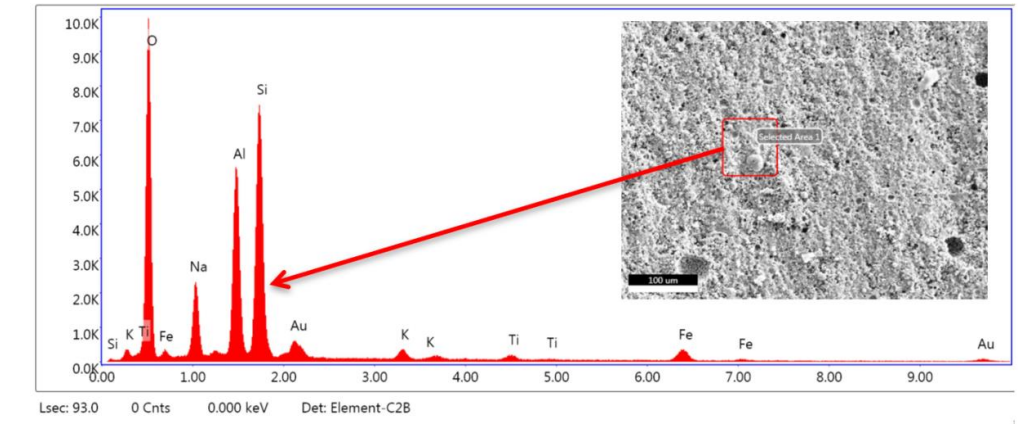

(b)

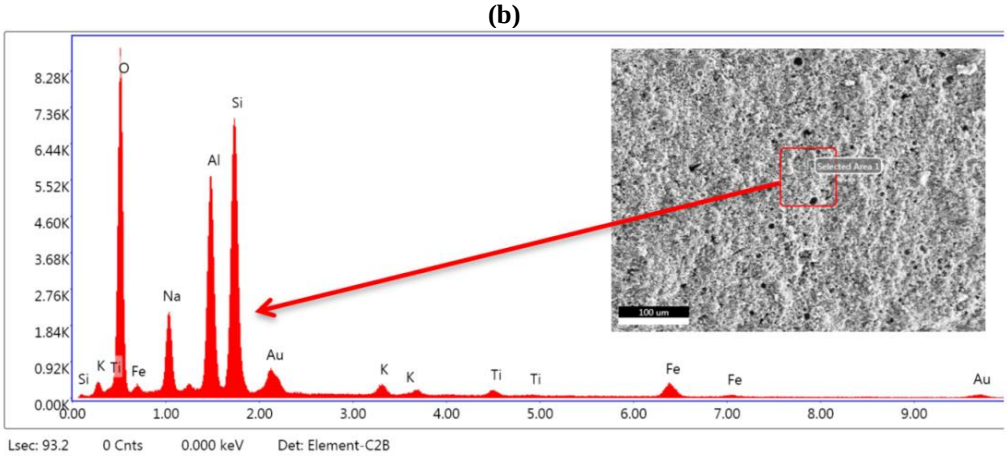

(c)

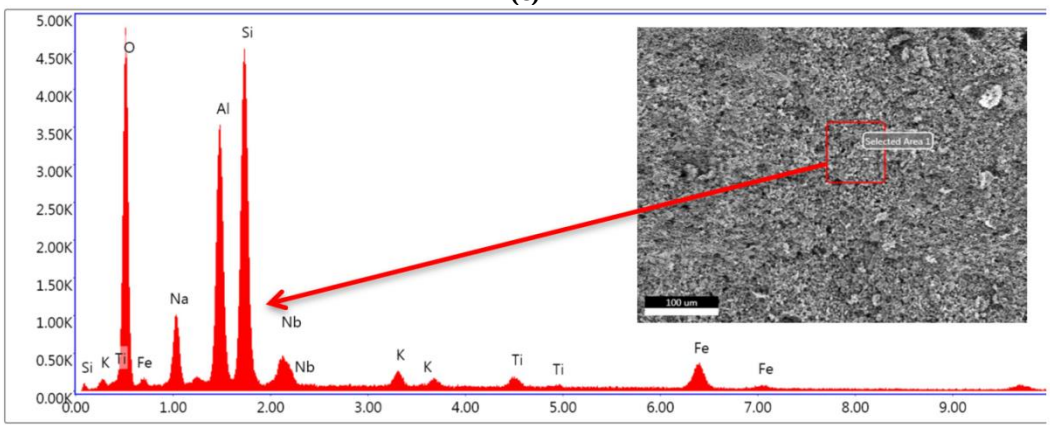

(d)

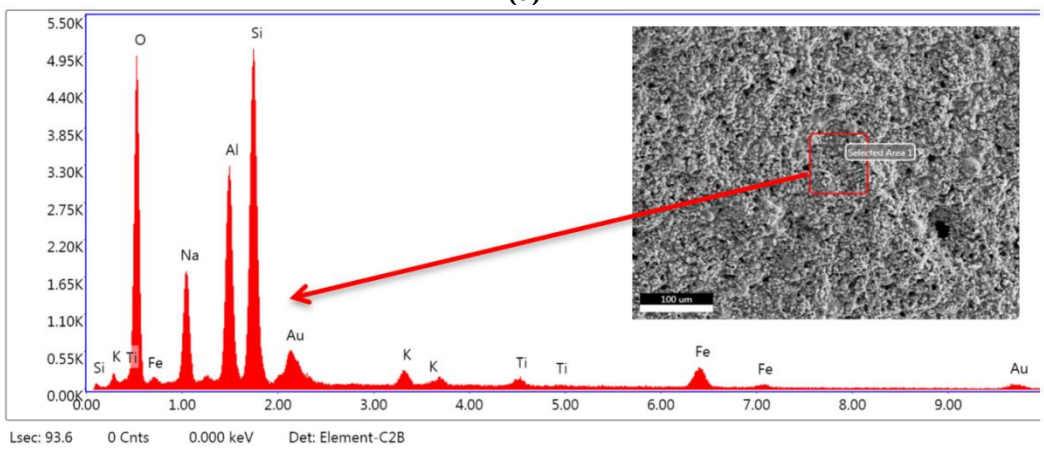

(e)

Figure 16. EDS spectra of geopolymer specimen ID 14MGP under exposure to high temperature: **(a)** 200°C; **(b)** 400°C; **(c)** 600°C; **(d)** 800°C; **(e)** 1000°C, respectively.

4. Conclusions

This present investigation investigated the effect of NaOH concentration on the mechanical and microstructural characteristics of fly ash-based geopolymer. The results have shown that the geopolymer specimen's mechanical properties increase with the NaOH concentration increase for up to a certain concentration, i.e., 14M, but show a reverse trend after that. So, it can be concluded that the concentration of alkaline solutions plays an important role in the mechanical strength development of geopolymer specimens. The geopolymer specimen ID 14MGP exhibits the highest compressive strength, flexural strength, and hardness value of 32 MPa, 6.3 MPa, and 67.84 HV, respectively. The SEM fractograph of geopolymer specimen ID 14MGP shows a dense geopolymer matrix, and the TEM fractograph confirms the formation of sodium aluminosilicate gel and hardened matrix. The FTIR spectra confirm the shifting of the peak from higher to lower wave numbers, indicating the formation of new products. Mineralogical analysis shows the major crystalline phase's presence in the parent materials, and the geopolymeric specimens are quartz and mullite, which form the main mineral framework attributed to the mechanical strength of the geopolymeric specimens. The geopolymer specimen ID 14MGP shows the lowest water absorption rate of 7.46 %. The mass loss of fly ash powder and geopolymeric specimen ID 14MGP is confirmed by the thermo gravimetric analysis (TGA). The residual compressive strength of the geopolymer specimen increased when the specimens were exposed to 200℃ but afterward decreased when exposed to high temperatures such as 400℃, 600℃, 800℃, and 1000℃ as compared to the reference optimized geopolymeric specimen. The specimen exposed to 1000℃ shows the lowest compressive strength of 0 MPa. Microstructural analysis confirms the formation of pores and cracks in the geopolymer specimen, which are responsible for the deterioration of compressive strength.

Funding

The work has received financial support from Govind Ballabh Pant National Institute of Himalayan Environment and Sustainable Development (IERP Project), Government of India, for funding the research project entitled ‘‘Production of Geopolymer based construction material from Fly ash: An industrial waste.’’ bearing grant no: GBPI/IERP/17-18/44 dated 28th March 2018.

Acknowledgments

The authors would like to thank the Central Instrumentation Center, Tripura University (A Central University), Agartala, Tripura, India, and the Department of Chemical and Polymer Engineering, Tripura University, Agartala, for the FESEM and FTIR facility.

Conflicts of Interest

The authors declare no conflict of interest.

References

1. Bell, S.E.; York, R. Coal, Injustice, and Environmental Destruction. *Organ. Environ.* **2012**, *25*, 359–367, https://doi.org/10.1177/1086026612468138.
2. Gajaje, K.; Ultra, V.U.; Nwaefuna, A.E.; Zhou, N. Phytostabilization of Fly Ash from a Coalmine in

Botswana and Biovalorisation of the Recovered Napier Grass (Pennisetum Purpureum Schumach.). *Int. J. Phytoremediation* **2024**, *26*, 1291–1304, https://doi.org/10.1080/15226514.2024.2313559.
3. Zierold, K.M.; Odoh, C. A Review on Fly Ash from Coal-Fired Power Plants: Chemical Composition, Regulations, and Health Evidence. *Rev. Environ. Health* **2020**, *35*, 401–418, https://doi.org/10.1515/reveh-2019-0039.
4. Roy, R.; Das, D.; Rout, P.K. A Review of Advanced Mullite Ceramics. *Eng. Sci.* **2022**, *18*, 20–30, https://doi.org/10.30919/es8d582.
5. Das, D. Role of Particle Size on the Mechanical and Microstructural Properties of Fly Ash-Based Geopolymer. *Interactions* **2024**, *245*, 277, doi:10.1007/s10751-024-02117-3.
6. Debnath, K.; Das, D.; Kumar Rout, P. Effect of Mechanical Milling of Fly Ash Powder on Compressive Strength of Geopolymer. *Mater. Today Proc.* **2022**, *68*, 242–249, https://doi.org/10.1016/j.matpr.2022.08.321.
7. Roy, R.; Das, D.; Rout, P.K. Fabrication of Mullite Ceramic by Using Industrial Waste. In Smart Cities; CRC Press: Boca Raton, **2022**; pp. 285–291, http://dx.doi.org/10.1201/9781003287186-13.
8. Das, D.; Gołąbiewska, A.; Rout, P.K. Geopolymer Bricks: The next Generation of Construction Materials for Sustainable Environment. *Constr. Build. Mater.* **2024**, *445*, 137876, doi:10.1016/j.conbuildmat.2024.137876.
9. Das, D.; Rout, P.K. Coal Fly Ash Utilization in India. In New Horizons for Industry 4.0 in Modern Business, Nayyar, A., Naved, M., Rameshwar, R., Eds.; Springer International Publishing: Cham, **2023**; pp. 233-251, https://doi.org/10.1007/978-3-031-20443-2_11.
10. ASTM C 618, Standard Specification for Coal Fly Ash and Raw or Calcined Natural Pozzolan for Use as a Mineral Admixture in Concrete, Annual Book of ASTM Standards. **2005**, https://doi.org/10.1520/C0618-00.
11. Das, D.; Rout, P.K. Utilization of Thermal Industry Waste: From Trash to Cash. *Carbon – Sci. Technol.* **2019**, *11*, 43–48.
12. Duxson, P.; Fernández-Jiménez, A.; Provis, J.L.; Lukey, G.C.; Palomo, A.; Van Deventer, J.S.J. Geopolymer Technology: The Current State of the Art. *J. Mater. Sci.* **2007**, *42*, 2917–2933, https://doi.org/10.1007/s10853-006-0637-z.
13. Lazorenko, G.; Kasprzhitskii, A. Geopolymer Additive Manufacturing: A Review. *Addit. Manuf.* **2022**, *55*, 102782, https://doi.org/10.1016/j.addma.2022.102782.
14. Panias, D.; Giannopoulou, I.P.; Perraki, T. Effect of Synthesis Parameters on the Mechanical Properties of Fly Ash-Based Geopolymers. *Colloids Surfaces A Physicochem. Eng. Asp.* **2007**, *301*, 246–254, https://doi.org/10.1016/j.colsurfa.2006.12.064.
15. Asadi, I.; Baghban, M.H.; Hashemi, M.; Izadyar, N.; Sajadi, B. Phase Change Materials Incorporated into Geopolymer Concrete for Enhancing Energy Efficiency and Sustainability of Buildings: A Review. *Case Stud. Constr. Mater.* **2022**, *17*, e01162, https://doi.org/10.1016/j.cscm.2022.e01162.
16. Hamidi, R.M.; Man, Z.; Azizli, K.A. Concentration of NaOH and the Effect on the Properties of Fly Ash based Geopolymer. *Procedia Eng.* **2016**, *148*, 189–193, https://doi.org/10.1016/j.proeng.2016.06.568.
17. Görhan, G.; Kürklü, G. The Influence of the NaOH Solution on the Properties of the Fly Ash-Based Geopolymer Mortar Cured at Different Temperatures. *Compos. Part B Eng.* **2014**, *58*, 371–377, https://doi.org/10.1016/j.compositesb.2013.10.082.
18. Gao, K.; Lin, K.-L.; Wang, D.; Hwang, C.-L.; Shiu, H.-S.; Chang, Y.-M.; Cheng, T.-W. Effects SiO2/Na2O Molar Ratio on Mechanical Properties and the Microstructure of Nano-SiO2 Metakaolin-Based Geopolymers. *Constr. Build. Mater.* **2014**, *53*, 503–510, https://doi.org/10.1016/j.conbuildmat.2013.12.003.
19. Castillo, H.; Collado, H.; Droguett, T.; Sánchez, S.; Vesely, M.; Garrido, P.; Palma, S. Factors Affecting the Compressive Strength of Geopolymers: A Review. *Minerals* **2021**, *11*, 1317, https://doi.org/10.3390/min11121317.
20. Moison, I.C.; Gungat, L.; Asrah, H.; Chiew, F.H. A Review of Eggshell Powder and Fly Ash-Based Geopolymers Concrete. *IOP Conf. Ser. Mater. Sci. Eng.* **2022**, *1229*, 012011, https://doi.org/10.1088/1757-899X/1229/1/012011.
21. Das, D. Role of Particle Size on the Mechanical and Microstructural Properties of Fly Ash-Based Geopolymer. *Interactions* **2024**, *245*, 277, https://doi.org/10.1007/s10751-024-02117-3.
22. Yuan, J.; He, P.; Jia, D.; Yang, C.; Zhang, Y.; Yan, S.; Yang, Z.; Duan, X.; Wang, S.; Zhou, Y. Effect of Curing Temperature and SiO2/K2O Molar Ratio on the Performance of Metakaolin-Based Geopolymers. *Ceram. Int.* **2016**, *42*, 16184–16190, https://doi.org/10.1016/j.ceramint.2016.07.139.

23. Das, D.; Gołąbiewska, A.; Rout, P.K. Geopolymer Bricks: The next Generation of Construction Materials for Sustainable Environment. *Constr. Build. Mater.* **2024**, *445*, 137876, https://doi.org/10.1016/j.conbuildmat.2024.137876.
24. Abdullah, M.M.A.; Kamarudin, H.; Mohammed, H.; Khairul Nizar, I.; Rafiza, A.R.; Zarina, Y. The Relationship of NaOH Molarity, Na2SiO3/NaOH Ratio, Fly Ash/Alkaline Activator Ratio, and Curing Temperature to the Strength of Fly Ash-Based Geopolymer. *Adv. Mater. Res.* **2011**, *328–330*, 1475–1482, https://doi.org/10.4028/www.scientific.net/AMR.328-330.1475.
25. Chindaprasirt, P.; Chalee, W. Effect of Sodium Hydroxide Concentration on Chloride Penetration and Steel Corrosion of Fly Ash-Based Geopolymer Concrete under Marine Site. *Constr. Build. Mater.* **2014**, *63*, 303–310, https://doi.org/10.1016/j.conbuildmat.2014.04.010.
26. Ghafoor, M.T.; Khan, Q.S.; Qazi, A.U.; Sheikh, M.N.; Hadi, M.N.S. Influence of Alkaline Activators on the Mechanical Properties of Fly Ash based Geopolymer Concrete Cured at Ambient Temperature. *Constr. Build. Mater.* **2021**, *273*, 121752, https://doi.org/10.1016/j.conbuildmat.2020.121752.
27. Hwang, C.-L.; Huynh, T.-P. Effect of Alkali-Activator and Rice Husk Ash Content on Strength Development of Fly Ash and Residual Rice Husk Ash-Based Geopolymers. *Constr. Build. Mater.* **2015**, *101*, 1–9, https://doi.org/10.1016/j.conbuildmat.2015.10.025.
28. Das, D.; Rout, P.K. Synthesis, Characterization and Properties of Fly Ash based Geopolymer Materials. *J. Mater. Eng. Perform.* **2021**, *30*, 3213–3231, https://doi.org/10.1007/s11665-021-05647-x.
29. Atiş, C.D.; Görür, E.B.; Karahan, O.; Bilim, C.; İlkentapar, S.; Luga, E. Very High Strength (120MPa) Class F Fly Ash Geopolymer Mortar Activated at Different NaOH Amount, Heat Curing Temperature and Heat Curing Duration. *Constr. Build. Mater.* **2015**, *96*, 673–678, https://doi.org/10.1016/j.conbuildmat.2015.08.089.
30. Suraneni, P.; Burris, L.; Shearer, C.R.; Hooton, R.D. ASTM C618 Fly Ash Specification: Comparison with Other Specifications, Shortcomings, and Solutions. *ACI Mater. J.* **2021**, *118*, 157–167, https://doi.org/10.14359/51725994.
31. Sarkar, M.; Maiti, M.; Malik, M.A.; Xu, S.; Li, Q.; Mandal, S. Influence of Metal Oxide (V2O5) in Recycled Waste Materials for Advanced Durable Construction Technology. *Constr. Build. Mater.* **2018**, *171*, 770–778, https://doi.org/10.1016/j.conbuildmat.2018.03.231.
32. Das, D.; Das, A.P.; Rout, P.K. Effect of Slag Addition on Compressive Strength and Microstructural Features of Fly Ash based Geopolymer. In Circular Economy in the Construction Industry; CRC Press: Boca Raton, **2021**; pp. 61–68, http://dx.doi.org/10.1201/9781003217619-9.
33. Xu, L.-Y.; Alrefaei, Y.; Wang, Y.-S.; Dai, J.-G. Recent Advances in Molecular Dynamics Simulation of the N-A-S-H Geopolymer System: Modeling, Structural Analysis, and Dynamics. *Constr. Build. Mater.* **2021**, *276*, 122196, https://doi.org/10.1016/j.conbuildmat.2020.122196.
34. Das, D.; Rout, P.K. Synthesis of Inorganic Polymeric Materials from Industrial Solid Waste. *Silicon* **2022**, *15*, 1771–1791, https://doi.org/10.1007/s12633-022-02116-5.
35. Somna, K.; Jaturapitakkul, C.; Kajitvichyanukul, P.; Chindaprasirt, P. NaOH-Activated Ground Fly Ash Geopolymer Cured at Ambient Temperature. *Fuel* **2011**, *90*, 2118–2124, https://doi.org/10.1016/j.fuel.2011.01.018.
36. Puertas, F.; Martínez-Ramírez, S.; Alonso, S.; Vázquez, T. Alkali-Activated Fly Ash/Slag Cements: Strength Behaviour and Hydration Products. *Cem. Concr. Res.* **2000**, *30*, 1625–1632, https://doi.org/10.1016/S0008-8846(00)00298-2.
37. Hanjitsuwan, S.; Hunpratub, S.; Thongbai, P.; Maensiri, S.; Sata, V. Cement & Concrete Composites Effects of NaOH Concentrations on Physical and Electrical Properties of High Calcium Fly Ash Geopolymer Paste. *Cement and Concrete Composites* **2014**, *45*, 9–14, https://doi.org/10.1016/j.cemconcomp.2013.09.012.
38. Pavithra, P.; Srinivasula Reddy, M.; Dinakar, P.; Hanumantha Rao, B.; Satpathy, B.K.; Mohanty, A.N. Effect of the Na_2SiO_3/NaOH Ratio and NaOH Molarity on the Synthesis of Fly Ash-Based Geopolymer Mortar. In Geo-Chicago; Proceedings; **2016**; pp. 336-344, https://doi.org/10.1061/9780784480151.034.
39. Nath, S.K. Geopolymerization Behavior of Ferrochrome Slag and Fly Ash Blends. *Constr. Build. Mater.* **2018**, *181*, 487–494, https://doi.org/10.1016/j.conbuildmat.2018.06.070.
40. Das, D.; Rout, P.K. A Review of Coal Fly Ash Utilization to Save the Environment. *Water, Air, Soil Pollut.* **2023**, *234*, 128, https://doi.org/10.1007/s11270-023-06143-9.
41. van der Merwe, E.M.; Mathebula, C.L.; Prinsloo, L.C. Characterization of the Surface and Physical Properties of South African Coal Fly Ash Modified by Sodium Lauryl Sulphate (SLS) for Applications in PVC Composites. *Powder Technol.* **2014**, *266*, 70–78, https://doi.org/10.1016/j.powtec.2014.06.008.

42. Khan, S.A.; Uddin, I.; Moeez, S.; Ahmad, A. Fungus-Mediated Preferential Bioleaching of Waste Material Such as Fly - Ash as a Means of Producing Extracellular, Protein Capped, Fluorescent and Water Soluble Silica Nanoparticles. *PLoS One* **2014**, *9*, e107597, https://doi.org/10.1371/journal.pone.0107597.
43. Chithambaram, S.J.; Kumar, S.; Prasad, M.M. Thermo-Mechanical Characteristics of Geopolymer Mortar. *Constr. Build. Mater.* **2019**, *213*, 100–108, https://doi.org/10.1016/j.conbuildmat.2019.04.051.
44. Nath, S.K.; Kumar, S. Role of Particle Fineness on Engineering Properties and Microstructure of Fly Ash Derived Geopolymer. *Constr. Build. Mater.* **2020**, *233*, 117294, https://doi.org/10.1016/j.conbuildmat.2019.117294.
45. Rożek, P.; Król, M.; Mozgawa, W. Spectroscopic Studies of Fly Ash-Based Geopolymers. *Spectrochim. Acta - Part A Mol. Biomol. Spectrosc.* **2018**, *198*, 283–289, https://doi.org/10.1016/j.saa.2018.03.034.
46. Kumar, S.; Kristály, F.; Mucsi, G. Geopolymerisation Behaviour of Size Fractioned Fly Ash. *Adv. Powder Technol.* **2015**, *26*, 24–30, https://doi.org/10.1016/j.apt.2014.09.001.
47. Alehyen, S.; Achouri, M.E.L.; Taibi, M. Characterization , Microstructure and Properties of Fly Ash-Based Geopolymer. *Journal of Materials and Environmental Sciences* **2017**, *8*, 1783–1796.
48. Nath, S.K.; Kumar, S. Reaction Kinetics of Fly Ash Geopolymerization: Role of Particle Size Controlled by Using Ball Mill. *Adv. Powder Technol.* **2019**, *30*, 1079–1088, https://doi.org/10.1016/j.apt.2019.03.003.
49. Liew, Y.M.; Kamarudin, H.; Mustafa Al Bakri, A.M.; Bnhussain, M.; Luqman, M.; Khairul Nizar, I.; Ruzaidi, C.M.; Heah, C.Y. Optimization of Solids-to-Liquid and Alkali Activator Ratios of Calcined Kaolin Geopolymeric Powder. *Constr. Build. Mater.* **2012**, *37*, 440–451, https://doi.org/10.1016/j.conbuildmat.2012.07.075.
50. Davidovits, J. Geopolymers Inorganic Polymeric New Materials. *J. Therm. Anal.* **1991**, *37*, 1633–1656, https://doi.org/10.1007/bf01912193.
51. Hui-Teng, N.; Cheng-Yong, H.; Yun-Ming, L.; Abdullah, M.M.A.B.; Ern Hun, K.; Razi, H.M.; Yong-Sing, N. Formulation, Mechanical Properties and Phase Analysis of Fly Ash Geopolymer with Ladle Furnace Slag Replacement. *J. Mater. Res. Technol.* **2021**, *12*, 1212–1226, https://doi.org/10.1016/j.jmrt.2021.03.065.
52. Farhana, Z.F.; Kamarudin, H.; Rahmat, A.; Al Bakri, A.M.M. The Relationship between Water Absorption and Porosity for Geopolymer Paste. *Mater. Sci. Forum* **2014**, *803*, 166–172, https://doi.org/10.4028/www.scientific.net/MSF.803.166.
53. Rashad, A.M.; Gharieb, M. An Investigation on the Effect of Sea Sand on the Properties of Fly Ash Geopolymer Mortars. *Innov. Infrastruct. Solut.* **2021**, *6*, 53, https://doi.org/10.1007/s41062-020-00421-9.
54. Sin, S.Y.A.; Kareem, Z. The Role of GGBFS as a Promoter for Un-Calcined Kaolinite Based (Hydrosodalite Based) Geopolymer. Proceedings of the International Integrated Pollution Prevention and Control Symposium, Karabuk, Turkey 1-3 April 2021; **2021**, https://doi.org/10.5281/zenodo.6588687.
55. Nergis, D.D.B.; Abdullah, M.M.A.B.; Sandu, A.V.; Vizureanu, P. XRD and TG-DTA Study of New Alkali Activated Materials Based on Fly Ash with Sand and Glass Powder. *Materials* **2020**, *13*, 343, https://doi.org/10.3390/ma13020343.
56. Cheng-Yong, H.; Yun-Ming, L.; Abdullah, M.M.A.B.; Hussin, K. Thermal Resistance Variations of Fly Ash Geopolymers: Foaming Responses. *Sci. Rep.* **2017**, *7*, 1–11, https://doi.org/10.1038/srep45355.
57. Kong, D.L.Y.; Sanjayan, J.G.; Sagoe-Crentsil, K. Comparative Performance of Geopolymers Made with Metakaolin and Fly Ash after Exposure to Elevated Temperatures. *Cem. Concr. Res.* **2007**, *37*, 1583–1589, https://doi.org/10.1016/j.cemconres.2007.08.021.
58. Yang, Z.; Mocadlo, R.; Zhao, M.; Sisson, R.D.; Tao, M.; Liang, J. Preparation of a Geopolymer from Red Mud Slurry and Class F Fly Ash and Its Behavior at Elevated Temperatures. *Constr. Build. Mater.* **2019**, *221*, 308–317, https://doi.org/10.1016/j.conbuildmat.2019.06.034.
59. Škvára, F.; Šcul, R.; Tišler, Z.; Skřičík, P.; Šmilauer, V.; Cílová, Z.Z. Preparation and Properties of Fly Ash-Based Geopolymer Foams. *Ceram. - Silikaty* **2014**, *58*, 188–197.
60. Ul Haq, E.; Kunjalukkal Padmanabhan, S.; Licciulli, A. Synthesis and Characteristics of Fly Ash and Bottom Ash based Geopolymers-A Comparative Study. *Ceram. Int.* **2014**, *40*, 2965–2971, https://doi.org/10.1016/j.ceramint.2013.10.012.
61. Kuri, J.C.; Majhi, S.; Sarker, P.K.; Mukherjee, A. Microstructural and Non-Destructive Investigation of the Effect of High Temperature Exposure on Ground Ferronickel Slag Blended Fly Ash Geopolymer Mortars. *J. Build. Eng.* **2021**, *43*, 103099, https://doi.org/10.1016/j.jobe.2021.103099.
62. Khan, M.N.N.; Sarker, P.K. Effect of Waste Glass Fine Aggregate on the Strength, Durability and High Temperature Resistance of Alkali-Activated Fly Ash and GGBFS Blended Mortar. *Constr. Build. Mater.* **2020**, *263*, 120177, https://doi.org/10.1016/j.conbuildmat.2020.120177.

63. Ranjbar, N.; Mehrali, M.; Alengaram, U.J.; Metselaar, H.S.C.; Jumaat, M.Z. Compressive Strength and Microstructural Analysis of Fly Ash/Palm Oil Fuel Ash based Geopolymer Mortar under Elevated Temperatures. *Constr. Build. Mater.* **2014**, *65*, 114–121, https://doi.org/10.1016/j.conbuildmat.2014.04.064.
64. Kürklü, G. The Effect of High Temperature on the Design of Blast Furnace Slag and Coarse Fly Ash-Based Geopolymer Mortar. *Compos. Part B Eng.* **2016**, *92*, 9–18, https://doi.org/10.1016/j.compositesb.2016.02.043.
65. Payakaniti, P.; Chuewangkam, N.; Yensano, R.; Pinitsoontorn, S.; Chindaprasirt, P. Changes in Compressive Strength, Microstructure and Magnetic Properties of a High-Calcium Fly Ash Geopolymer Subjected to High Temperatures. *Constr. Build. Mater.* **2020**, *265*, 120650, https://doi.org/10.1016/j.conbuildmat.2020.120650.
66. Behera, P.; Baheti, V.; Militky, J.; Louda, P. Elevated Temperature Properties of Basalt Microfibril Filled Geopolymer Composites. *Constr. Build. Mater.* **2018**, *163*, 850–860, https://doi.org/10.1016/j.conbuildmat.2017.12.152.
67. Omer, S.A.; Demirboga, R.; Khushefati, W.H. Relationship between Compressive Strength and UPV of GGBFS Based Geopolymer Mortars Exposed to Elevated Temperatures. *Constr. Build. Mater.* **2015**, *94*, 189–195, https://doi.org/10.1016/j.conbuildmat.2015.07.006.
68. Luhar, S.; Chaudhary, S.; Luhar, I. Thermal Resistance of Fly Ash based Rubberized Geopolymer Concrete. *J. Build. Eng.* **2018**, *19*, 420–428, https://doi.org/10.1016/j.jobe.2018.05.025.
69. Moutaoukil, G.; Alehyen, S.; Sobrados, I.; el Mahdi Safhi, A. Effects of Elevated Temperature and Activation Solution Content on Microstructural and Mechanical Properties of Fly Ash-Based Geopolymer. *KSCE J. Civ. Eng.* **2023**, *27*, 2372–2384, https://doi.org/10.1007/s12205-023-1102-0.
70. Azimi, E.A.; Abdullah, M.M.A.B.; Vizureanu, P.; Salleh, M.A.A.M.; Sandu, A.V.; Chaiprapa, J.; Yoriya, S.; Hussin, K.; Aziz, I.H. Strength Development and Elemental Distribution of Dolomite/Fly Ash Geopolymer Composite under Elevated Temperature. *Materials* **2020**, *13*, 1015, https://doi.org/10.3390/ma13041015.
71. Ahmari, S.; Zhang, L. 13 - The properties and durability of mine tailings-based geopolymeric masonry blocks. In Eco-Efficient Masonry Bricks and Blocks, Pacheco-Torgal, F., Lourenço, P.B., Labrincha, J.A., Kumar, S., Chindaprasirt, P., Eds.; Woodhead Publishing: Oxford, **2015**; pp. 289-309, https://doi.org/10.1016/B978-1-78242-305-8.00013-9.